MODELING OF FLUID -VAPOR INTERFACE IN THE CONDENSATION ZONE OF A GROOVED HEAT PIPE

A THESIS SUBMITTED TO
THE GRADUATE SCHOOL OF NATURAL AND APPLIED SCIENCES
OF
MIDDLE EAST TECHNICAL UNIVERSITY

BY

MOBIN ALIPOUR

IN PARTIAL FULFILLMENT OF THE REQUIREMENTS
FOR
THE DEGREE OF MASTER OF SCIENCE
IN
MECHANICAL ENGINEERING

SEPTEMBER 2017

Approval of the thesis:

MODELING OF FLUID -VAPOR INTERFACE IN THE CONDENSATION ZONE OF A GROOVED HEAT PIPE

submitted by **MOBIN ALIPOUR** in partial fulfillment of the requirements for the degree of **Master of Science in Mechanical Engineering Department, Middle East Technical University** by,

Prof. Dr. Gülbin Dural Ünver
Dean, Graduate School of **Natural and Applied Sciences** _____

Prof. Dr. Raif Tuna Balkan
Head of Department, **Mechanical Engineering** _____

Prof. Dr. Zafer Dursunkaya
Supervisor, **Department of Mechanical Engineering, METU** _____

Examining Committee Members:

Assoc. Prof. Dr. Cuneyt Sert
Department of Mechanical Engineering, METU _____

Prof. Dr. Zafer Dursunkaya
Department of Mechanical Engineering, METU _____

Assist. Prof. Dr. Özgür Bayer
Department of Mechanical Engineering, METU _____

Prof. Dr. Serkan Özgen
Department of Aerospace Engineering, METU _____

Assoc. Prof. Dr. Barbaros Çetin
Department of Mechanical Engineering, Bilkent University _____

Date: ***September 6, 2017***

I hereby declare that all information in this document has been obtained and presented in accordance with academic rules and ethical conduct. I also declare that, as required by these rules and conduct, I have fully cited and referenced all material and results that are not original to this work.

Name, Last Name: MOBIN ALIPOUR

Signature :

ABSTRACT

MODELING OF FLUID -VAPOR INTERFACE IN THE CONDENSATION ZONE OF A GROOVED HEAT PIPE

Alipour, Mobin

M.S., Department of Mechanical Engineering

Supervisor : Prof. Dr. Zafer Dursunkaya

September 2017, 75 pages

Condensation in grooved heat pipes involves several simultaneous phenomena including vapor-liquid boundaries whose shapes are unknown *a priori*, fluid flow due to capillary and dispersion pressure gradients and condensation over ultra thin films. In grooved heat pipes, the majority of condensation occurs on fin tops due to the thinner liquid film, having a lower thermal resistance, compared to inside the groove where the fluid is substantially thicker. Majority of the studies in the literature assume an approximate profile for the liquid film surface and apply an integral balance for conservation laws, including the effect of the capillary pressure only. In addition, this approximate profile is matched with the liquid profile inside the groove, which serves as a boundary condition. In the current study, the effect of a slope dependent disjoining pressure and the matching conditions with the groove are investigated using a comprehensive model. The results suggest that for small temperature differences and small slopes, the effect of dispersion pressure is non negligible and beyond limiting values of edge slope angles, the disjoining effect precludes solutions where the

fin top film matches the groove in a smooth transition. In addition bifurcation manner is found for the results. Their physical availability is examined in this study. This analysis results suggested that the second set of answers which is found because of bifurcation, despite its mathematical validity, could not be physically valid.

Keywords: Condensation, micro-grooved heat pipe, disjoining pressure, micro region

ÖZ

OLUKLU BİR ISI BORUSUNUN YOĞUNLAŞMA BÖLGESİNDE SIVI -BUHAR ARAYÜZÜNÜN MODELLENMESİ

Alipour, Mobin
Yüksek Lisans, Makina Mühendisliği Bölümü
Tez Yöneticisi : Prof. Dr. Zafer Dursunkaya

Eylül 2017 , 75 sayfa

oluklu ısı borularındaki yoğunlaşma, şekilleri önceden bilinmeyen buhar-sıvı sınırları, kılcal damlacıklara ve dağılım basınç gradyenlerine bağlı sıvı akışı ve ultra ince filmler üzerindeki yoğunlaşma da dahil olmak üzere birçok eşzamanlı olayı içerir. oluklu ısı borularında yoğunlaşmanın çoğunluğu, sıvının daha kalın oldoğu oluk içinedençok, daha düşük ısıl direnci olan daha ince sıvı film nedeniyle kanatçık yuzuyında oluşur. Literatürdeki çalışmaların büyük bir çoğunluğu sıvı film yüzeyi için bir yaklaşık profil kullanarak ve yalnızca kılcal basınç etkisi ile koruma yasaları için bir denge uygular. Buna ek olarak, bu yaklaşık profil, oluk içindeki sıvı profili ile eşleştirilir, bu da bir sınır durumu şartı yerıne geçer. Bu çalışmada, eğime bağlı ayrılma basıncının etkisi ve eşleme koşulları ile kapsamlı bir model kullanılarak araştırılmıştır. Sonuçlar, küçük sıcaklık farkları ve duşuk eğimler için dağılma basıncının önemsiz olmadığı ve kenar eğim açılarındaki sınırlayıcı değerlerin ötesinde, ayrışan etki, kanatçık üstundeki filminin olukla eşleştiği yerlerde yumuşak bir geçişte bulunulduğunu önermektedir. Buna ek olarak, sonuçlar için bifürkasyon görülmüş ve bunun fiziksel sonuçları ince-

lenmiştir. Sonuçların bu analizi, bifurkasyon nedeniyle matematiksel geçerliliğine rağmen ikinci sonuç kümesinin fiziksel geçerliliğini incelemektedir.

Anahtar Kelimeler: Yoğunlaşma, mikro oluklu ısı borusu, ayrışma basıncı, mikro bölge

To my beloved parents and sister...

ACKNOWLEDGMENTS

I would like to thank Prof. Dr. Dursunkaya for his great support during my study. I benefit from his precious ideas which helped me to finalize this research. I learned how to start, progress and finalize an academic research in a correct way because of my adivisors guidance and I am utterly thankful for his helps.

I would like to thank my beloved family because of their invaluable supports. Always and in every single step of my life, I felt their full support and they never left me alone with difficulties. One of my main goals in life is to make them happy and feel them proud. I hope this will happen someday.

I would like to thank my sweetheart from the bottom of my heart. Schatzy gave me a pure and peaceful happiness during last 6 months with her eyes, laughter and words. I hope, I will never see her eyes sad during my life.

I would like to thank my friends for their support during these years; Ali farid, Frazad shams ,salar rahimi and roshan arianfar. I would like to thank arsalan javanmard whose friendship with me is a precious part of my life.

This study is financially supported by the Turkish Scientific and Technical Research Council, under grant No. 213M351.

TABLE OF CONTENTS

LIST OF TABLES

TABLES

LIST OF FIGURES

FIGURES

LIST OF ABBREVIATIONS

A	Dispersion constant, J
c	accommodation constant
h_{lv}	Latent heat of evaporation, J/kg
k_l	Thermal conductivity, W/m.K
M	Molar mass of liquid, kg/mol
m'	Mass flow rate, kg/s
n	Number density of molecule,m^-3
L_c	Lagrange multiplier
P_c	Capillary pressure, Pa
P_d	disjoining pressure, Pa
P_l	Liquid pressure, Pa
P_v	Vapor pressure, Pa
q''	Heat flux, W/m^2
R_u	Universal gas constants, j/mol.K
V_l	Molar volume of liquid, m^3/mol
T_l	Liquid temperature, K
T_{lv}	Liquid-vapor inter-facial temperature, K
T_v	Vapor temperature, K
ΔT	Temperature difference between vapor and liquid, C
x^*	Half length of the droplet
	Greek Symbols
β_{ff}	Strength of van der Waals potentials between fluid-fluid molecules.
β_{fg}	Strength of van der Waals potentials between fluid-gas molecules.
β_{fs}	Strength of van der Waals potentials between fluid-solid molecules.
δ	Film thickness, m
$\bar{\delta}$	Variation of function

μ	Dynamic viscosity, Pa.s
ν	Kinematic viscosity, m^2/s
ρ	Density, kg/m^3
σ	Surface tension, N/m
σ_{fg}	Liquid-vapor surface tension, N/m
σ_{fs}	Liquid-solid surface tension, N/m
σ_{sg}	Solid-vapor surface tension, N/m

CHAPTER 1

INTRODUCTION

Electrical devices contain multiple smaller parts with noticeable amount of heat dissipation. Performance and efficiency of an electrical system relies on some dependent factors. One of them is cooling process of the components and thermal management of the whole system. Phase change process enables the heat pipes to transfer the heat from heat source to sink with smaller distance and lower temperature differences. This is mainly because of the large amount of heat winch phase change requires in order to be happened. Traditional and commonly used cooling methods are not able to address the high heat concentrated components which modern electrical devices contain. Alternative replacement of this traditional cooling systems could be design by focusing on using phase change process which will make them applicable for this cited cooling cases. An example of systems benefiting from phase change is heat pipe. Heat pipes are comprise a container which includes three zones; evaporation, condensation and adiabatic. Pressure gradient caused because of the capillary pressure difference inside the container of the heat pipes, enables the condensed liquid to flow from condensation to evaporation section. In order to have a physical representation, the phase change phenomena of evaporation and condensations should accurately modeled. Intermolecular forces and interactions becomes dominant in the scale of the thin liquid films. These ultra thin fluid layers encountered in phase change process, should be modeled by considering the intermolecular forces in order to have a more accurate predictions for the scale of the liquid film and consequently on the thermal behavior of the heat pipe.

1.1 Heat pipe

Heat pipes include a container, wick structure and a operational liquid. Heat pipe has three main zones; condensation, evaporation and adiabatic region. Heat is transferred from the heat source outside the container to the operating liquid, this caused the liquid to evaporate. This region where the phase change from liquid to vapor happens is called evaporation zone. In the heat sink zone, by observing the heat from the heat pipe, the vapor condensed to liquid. This part of the heat pipe is named condensation zone. The region between evaporation and condensation parts, is the adiabatic zone in which the thermal transfer is not happening. It should be noted that the exact location of the adiabatic region is not clear which means the exact distinguishing limit between this transition section and evaporation or condensation zone is unknown. The schematic of the heat pipe and its mechanism is shown in Fig. 1.1.

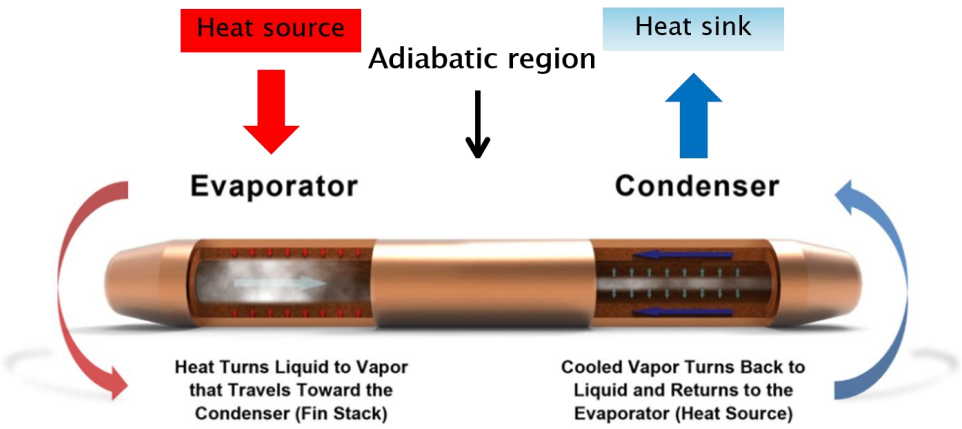

Figure 1.1: Schematic of the heat pipe, picture adopted from[1]

Transport mechanism of the liquid inside the container from condensation to the evaporation zone which allows the heat pipe to operate with out delay, is supplied by the wick structure. This structure allows the water to flow back to the evaporation zone by using the capillary pressure differences which is emerged and became dominant because of the wick structure. This wick structured could be implemented to the container with different methods like creating grooves or adding sinter.

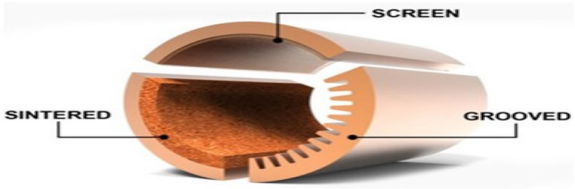

Figure 1.2: Two different methods for creating Wick structure[1]

1.1.1 Types of heat pipes

The simplest form of heat pipes are traditional cylindrical models. Theses models include a container with cylindrical cross section and different kinds of wick structures which are chosen based on their applications. An another type of heat pipe which due to its geometry is more applicable for electronic devices, is flat heat pipe. In this kind of heat pipe the cross section of the container is rectangular, despite the cylindrical models, but the working mechanism of both are almost similar. Capillary pumped looped heat pipes are the most widely used heat pipes for spacecraft applications. The schematic of its structure is presented in Fig. 1.5. It benefits from the two-phase reservoir which enables the heat pipe to control the working fluid and the temperature. Another form of the heat pipes which could have a noticeable potential for cooling application of the electronic devices, are micro and miniature heat pipes. The micro heat pipe was defined as a heat pipe in which the mean curvature of the liquid vapor interface is comparable in magnitude to the reciprocal of the hydraulic radius of the total flow channel [2]. If the hydraulic diameter of the heat pipe is in the range of 0.5 - 1.5 mm, it could be named as miniature heat pipe [6]. Differentiation between miniature and micro heat pipes are not well defined in the literature. For instance, in some papers, miniature heat pipes including several micro grooves are named as micro heat pipe either Fig. 1.5.

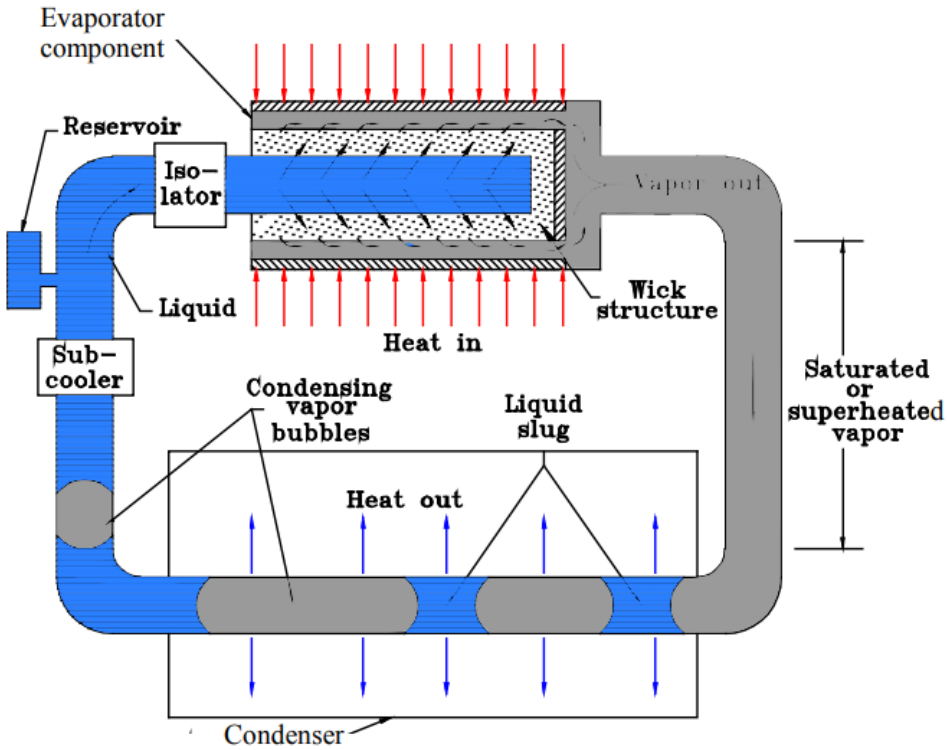

Figure 1.3: Capillary pumped loop heat pipe [2]

1.2 Physical phenomena of phase change

Phase change is the principal physical mechanism of transformation between one thermodynamic state to a new one. Some phenomena related to phase change is explained in this section.

1.2.1 Phase change

The advantage that help heat pipes to remove the heat in shorter distance and with lower temperature difference between the heat source and sink, is phase change. Two phase change mechanism happen in the container; evaporation and condensation. The both of them play a great role in the heat removal process. In micro grooved heat pipes, evaporation mostly happens in the liquid-solid interface inside the groove just before the edge of the fin. Despite the evaporation, condensation mostly occurs on the fin top where the liquid thickness is

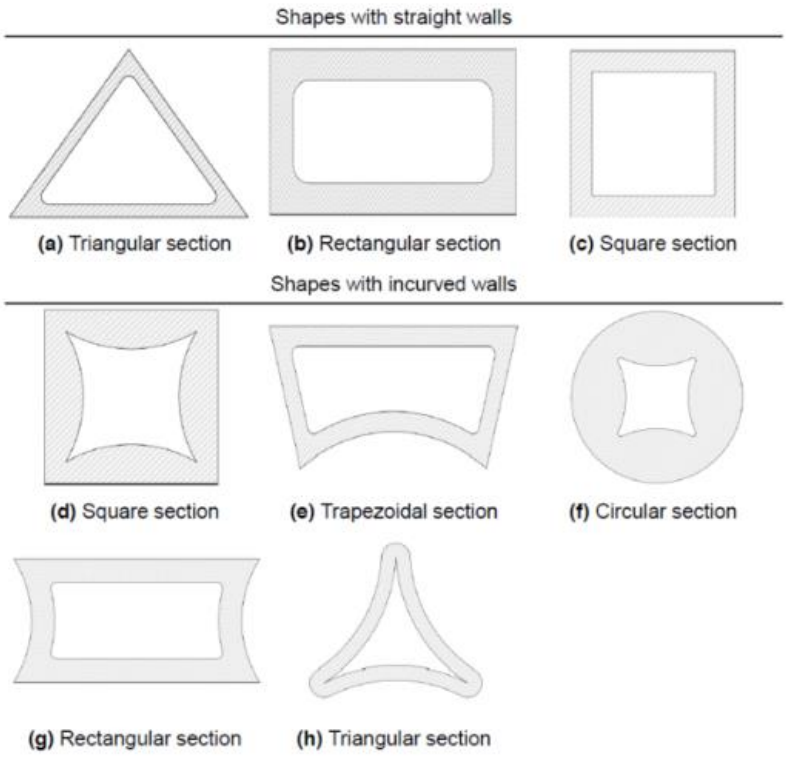

Figure 1.4: Different micro heat pipe cross sections [3]

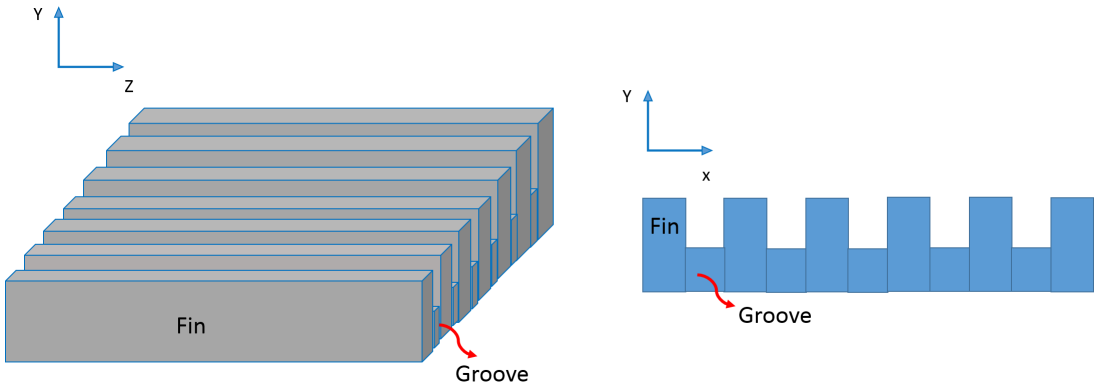

Figure 1.5: grooved heat pipes cross sectional views

thinner than the liquid inside the groove. The schematic of the evaporation and condensation sections in the heat pipe are shown in Fig. 1.6. Since the condensation modeling is taken into consideration in this study, a brief introduction of it is presented in this section.

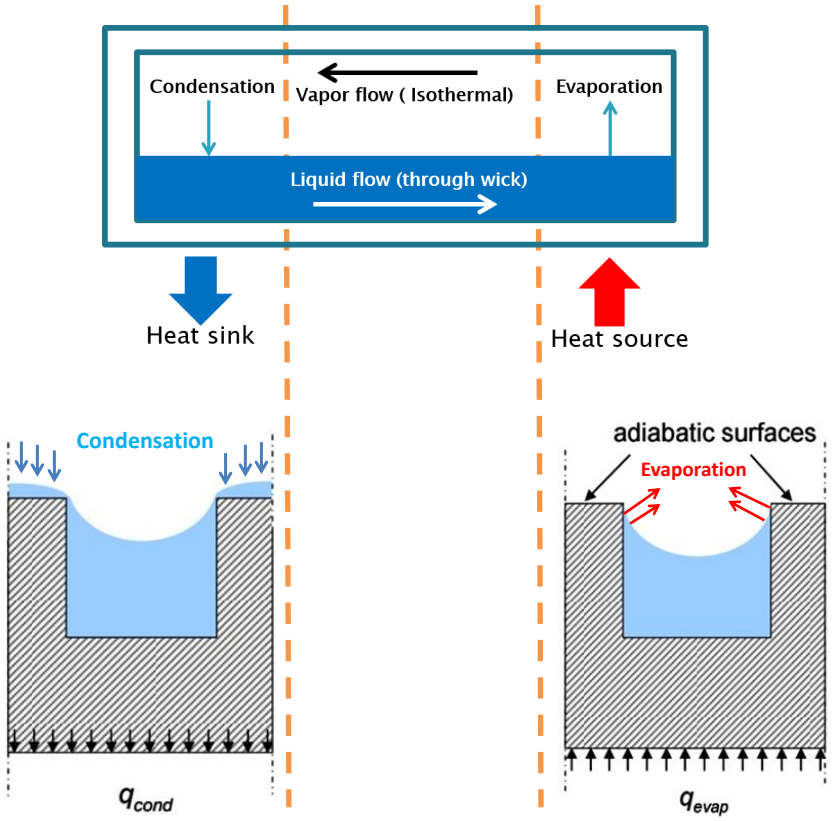

Figure 1.6: Cross sectional view of the condensation and evaporation phase change process in micro grooved heap pipe, figure partly adapted from [5]

1.2.1.1 Condensation and evaporation

Condensation is a phase change process in which gas converts to liquid, and is the reverse process of the evaporation. In order to have a better modeling calculation of the mass flux created because of the condensation or evaporation, in addition of the thermal difference, pressure balance between two phases should be analyzed. At liquid-vapor interface, mass, momentum and energy conservation should be satisfied in the condensation modeling. Energy balance of the condensation and evaporation could be written as

$$q_l'' - q_v'' = m_c'' h_l v. \tag{1.1}$$

Conservation of momentum reduces to augmented Young-Laplace equation and is expressed as

$$P_v - P_l = P_c + P_d \tag{1.2}$$

where P_v, P_l, P_c and P_d refers to vapor, liquid, capillary and disjoining pressure respectively.

1.2.1.2 Capillary pressure

Surface tension generated from deformation of the interface curvature, results in the presence of the capillary pressure. It is a function of radius of the film and surface tension. Since the radius of the liquid inside the groove is much larger than the liquid on the fin top, the related term could be neglected and the final form of the capillary pressure for the condensation liquid film is reduced to

$$P_c = \frac{\sigma}{R} \tag{1.3}$$

where R could be written as a function of the film curvature and expressed as

$$P_c = \frac{\sigma \delta_{xx}}{\left(1 + {\delta_x}^2\right)^{3/2}}. \tag{1.4}$$

1.2.1.3 Disjoining pressure

In the thin film layers, less than 100 nm, inter molecular interactions mostly caused by van der Waals forces, become dominant. In order to remove a small increment of this thin layer, an equilibrium force is required which its magnitude depends on the layers thickness and caused by the pressure which is named as disoining pressure. Disjoinig pressures effect is dominant in modeling of droplets and thin layers of liquid films and it should be included in the mathematical modeling of these problems.

1.3 Scope of the Thesis

In this study condensation film is modeled by considering the conservation of mass and momentum along with the augmented Young-Laplace equation which is solved numerically while the effect of slope and curvature dependent disjoining pressure is included in the calculation process. Beside this model, the 4^{th} order polynomial fitting approach and the case in which the disjoining pressure is neglected, are taken into consideration and compared. Validity of the boundary conditions especially those related to the edge of the fin top are discussed and compared with the experimental results available in literature and the results dependency to the different effective parameters are presented. State of art review of the condensation and evaporation modelings is presented in chapter 2. Chapter 3 refers to the modeling process of fluid flow and condensation process. In this chapter, numerical approach that is used in this study in order to solve the condensation films general equation is discussed. Results and discussions are presented in chapter 4. Finally, conclusion and future works are discussed and suggested in chapter 5.

CHAPTER 2

LITERATURE REVIEW

Thin liquid meniscus inside the groove and in the evaporation region, has been modeled by numerous studies in the past decades. Potash and Wayner [7] presented a mathematical model of the evaporation for the extended meniscus in 1972. Prior to this study, Wayner et al. [8] suggested the transport model by considering the disjoining pressure for the thin liquid film on a flat plate. In 1976 Wayner et al. [9] modified the Schrage [10] for phase change by including the Clausius-Clapeyron equation and the equation given by Derjaguin[11]. In this study evaporation mass flux was expressed as a function of the pressure and temperature jump and the fluid flow assumed to behave as a 1-D lubrication flow. These cited assumptions and considerations were further used by various studies in literature. Mirzamoghadam et al. [12] applied appropriate profiles for temperature and velocity distributions in order to model the menisci of evaporation in a way similar to boundary layer methods. Dasgupta et al. [13] modeled dispersion and capillariy forces to be continuous by including the augmented Young-Laplace equation in the modeling, but variation in the film thickness was assumed to be small and neglected which renders the model invalid in case of highly curved menisci. Stephan and Busse [14], unlike the other studies mentioned above, conducted a mathematical modeling based on combining conservation equations of mass and momentum and solving the resulting ODE by Runge-Kutta numerical scheme. They asserted that assuming the same temperature for the interfacial and saturation temperatures could result in over prediction of heat transfer coefficient. Wee et al. [15] and Wang et al. [16] used the same solution methodology as the one used in [14]. Wee et al. [15] analyzed the polarity of the liquid and concluded that polarity leads to

the reduction of evaporation rate due to the increase in the van der Waals forces of polar liquid. In contrast to what was assumed in [9] about the equality of the temperature of the bulk vapor and the vapor in the vicinity of the liquid-vapor interfacial line which were both included in the mass flux, Wang et al. [16] did not consider this assumption. It was found that this assumption results in an underestimation of the heat transfer coefficient for superheats more than 5 K. Wang et al. [16] also emphasized the importance of the sharing rate of micro region in the total heat transfer rate of the evaporation meniscus. Another research which used the same methodology as what Stephan and Busse[14] applied in their model, is a study that was conducted by Bertossi et al. [17]. This research was based on a parametric study and uttered that contact angle and intrinsic meniscus region are totally independent. In 2011, Du and Zhao [18] introduced new boundary conditions for the numerical solution of the initial differential equation of the evaporation region, with the same methodology as what was presented by Wang et al. [16]. In 2015 Kou et al. [19] compared the effects of applying different formulation of evaporation mass flux to the evaporation modeling and discussed their results. Wayner and Clausius–Clapeyron formulation for evaporation mass flux were both considered and discussed in this research. A novel approach for solving the mathematical modeling of the evaporation in order to find the more accurate meniscus profile is presented by Akkuş and Dursunkaya[21] in 2016. In this study, starting point for solving the differential equation was located in the intrinsic meniscus region where the ratio of disjoining pressure to capillary pressure was significant and the results were compared with the results of Stephan and Busse [14]. Evaporation modeling inside the grooved heat pipe has been studied noticeably more in comparison of condensation modeling. Evaporation mostly happens on edge of fin and groove, but most of the condensation happens on the fin top and its magnitude inside the groove is negligible. This is due to the thinner thickness of the liquid fim on the fin top. In 2001, Zhang and Faghri [4] modeled the condensation film inside the groove and on the top of the fin of the rectangular shaped groove by using VOF method. Forces due to the pressure jump at the liquid-vapor interface were modeled as volume force by using divergence theorem and finally Effects of contact angle, surface tension and fin geometry were discussed. They stated

that convection has negligible effect on the condensation liquid film and it can be excluded form the modeling process. Also, the assumption that most of the condensation happens on the fin top was confirmed based on the results of their modeling. In the study of Jiao et al. [22] which was conducted in 2005, thick-

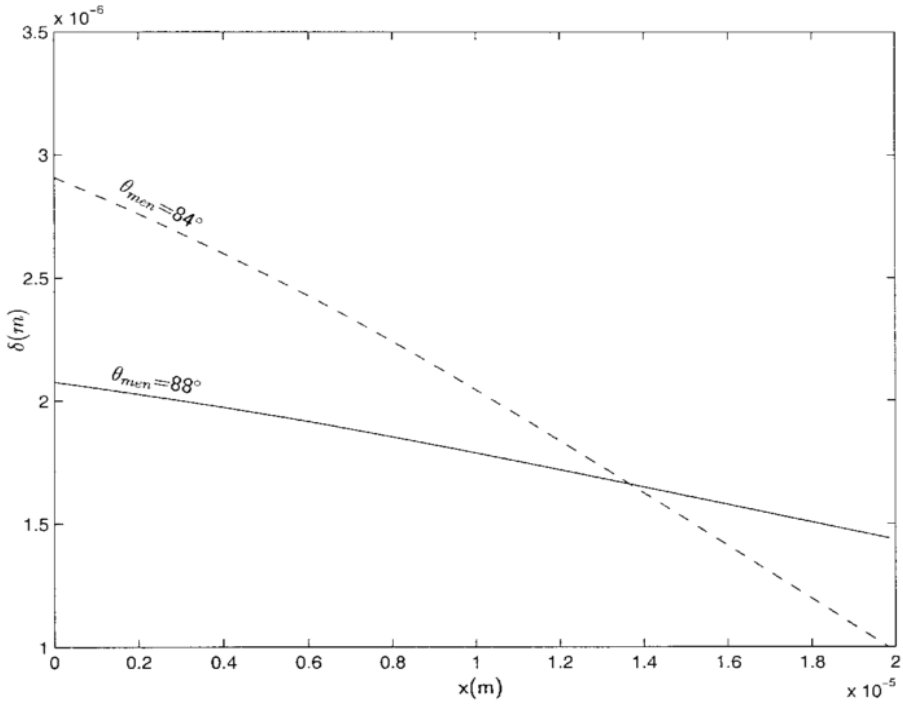

Figure 2.1: Predictions for condensation film presented in[4]

ness of liquid film was assumed to be constant. A hydrodynamic model for the flow on the fin top created because of condensation was presented in this study. A hydrodynamic model which its governing equation was based on coupling four nonlinear ODEs which were derived from conservation of mass, momentum and cosnidering Young-Laplace equation, was reported by [5, 23]. They used Runge-Kutta numerical method for solving the governing equation and Disjoining pressure was neglected in this study. Condensation mass flux was assumed to be constant along the fin top by using Clausius-Clapeyron formulation and the liquid film on the fin top was considered to be symmetric. Four boundary conditions were assumed in this research, two satisfying the contact angle at the fin top and the symmetric condition at the beginning, the other two boundaries refer to the magnitude of the velocity, and the pressure of liquid being equal to

vapor pressure at the fin edge. Furthure, The results of the flow modeling and film thickness predictions was coupled to the two dimensional thermal model in their study. In 2010, they reported a comparison between theoretical results and experimental observations [5]. The experimental observation which is reported in their study, shows a significant difference between the theoretical predictions of condensation film on the fin top and the experimental data. In addition, the observed profile contain one change in the slope of the liquid film before the edge, where the authors named it as slope break. This change in slope does not happen in theoretical models predictions. It was mentioned that the exact lo-

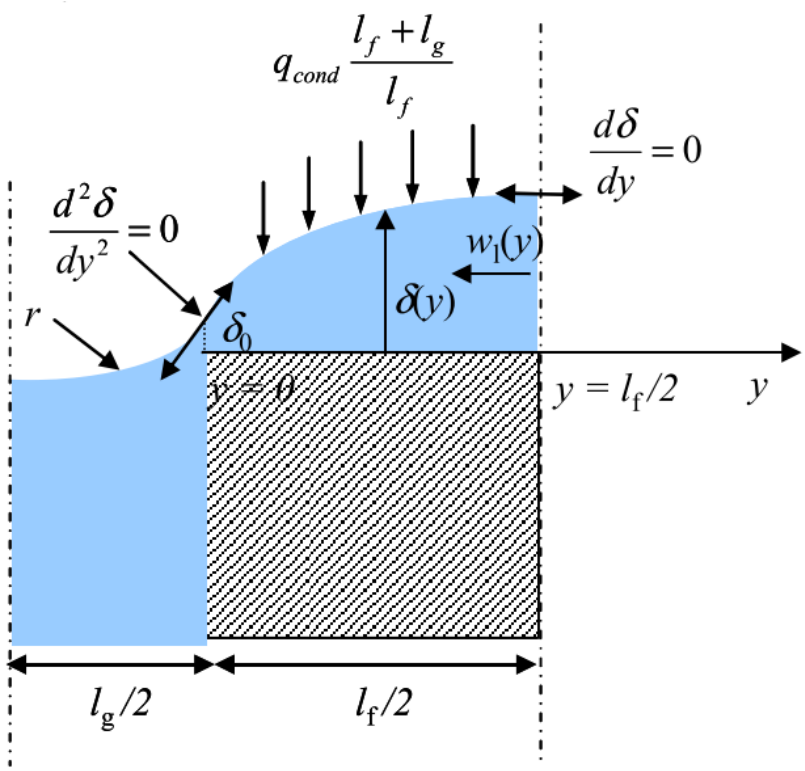

Figure 2.2: Boundary conditions used in [5] for the modeling of condensation film

cation of the fin edge was not clear for them during the test and maybe it could bring some errors for results. This cited slope break and difference between results should be taken into consideration. The possible reasons attributed to this mentioned slope break was asserted by authors as: (i) van der Waals forces and intermolecular interactions at the fin edge where the thickness of the liquid film is extremely thin could effected the film profile and it was neglected in their modeling. (ii) flow could also be in the parallel direction of the groove on the

fin top which is neglected in the modeling.

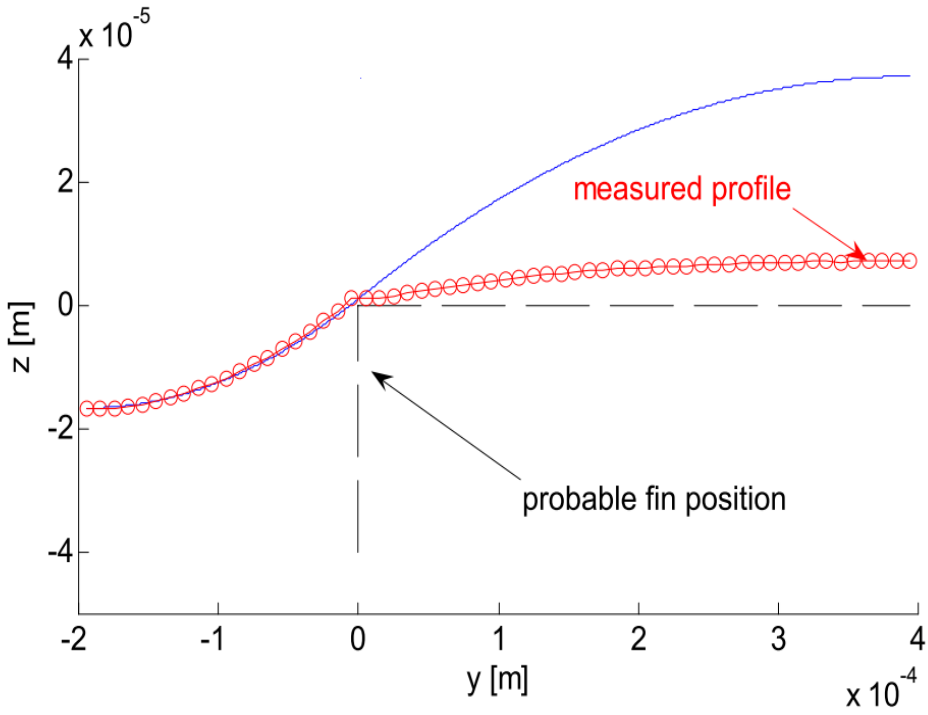

Figure 2.3: Comparison of theoretical and experimental results for condensation film in [5]

In 2008 and 2010, a method for predicting the approximated film profile of the condensed liquid on the fin top was introduced by Do et al. [20, 24]. This method was based on fitting a 4^{th} order polynomial to the governing equation derived from conservation of mass, momentum and Young-Laplace equation. This derivation resulted in one single differential equation that was function of film profile. The same method was used by Odabaşi [25] in 2014 for modeling the condensation film. Wayner's formulation for evaporation and condensation mass flux is implemented by different researches for modeling the fluid-vapor interface [3, 9, 13, 15, 16, 18–21, 24–33], on the other hand, Clausius–Clapeyron formulation is applied by other researches as the main method for calculating the evaporation and condensation interfacial mass flux for their modeling [5, 12, 14, 17, 19, 23, 34, 35].

Effect of disjoining pressure on the behavior of the evaporation menisci was discussed by diffrent researchers, but it was not considered as a part of con-

densation modeling. In 1957, Derjaguin and Zorin [11] described the concept of the disjoining pressure and presented experimental data for polar liquids, which were formulated as a logarithmic function by Holm and Goplen [36] in 1979. Derjaguin and Zorin [11] also introduced the polynomial which was only function of film thickness for calculating the disjoining pressure of the non-polar liquids. These mentioned formulas are commonly used in the literature to include the effects of the disjoining pressure in the evaporation modeling for both polar and non-polar liquids[9, 13, 15–21, 26–28, 31, 34]. All the cited efforts for applying disjoining pressure used the formula which is solely dependent on the film thickness and independent of the slope and curvature of the film profile. Hocking [37] suggested an expression which contains derivatives of the film thickness, however, this expression has two major problems; (i) this expression was derived by assuming a constant intermolecular potential along the liquid-vapor interface, and it does not satisfy the equilibrium condition because the intermolecular potentials of the inside of the droplet or film was not taken into account. (ii) The second problem refers to the assumption that Hocking [37] took by equaling the disjoining pressure with the intermolecular potential at the interface, which is utterly unjustified. Indeikina and Chang [38] tried a similar approach and derived a slope dependent disjoining pressure, but the total equilibrium condition was not satisfied in their research either. In 2004, Wu and Wang [39] expressed a new slope and curvature dependent disjoining pressure, which is modified for small variations of fluid film—i.e. small slopes—and derived by analyzing the equilibrium condition. In this research study, an equilibrium condition was derived from minimizing the total energy of a droplet on a substrate in which intermolecular interactions and resulting excess energy is included. This formulation includes higher order terms which prevent a contact line from moving without slip when a liquid film ends at a substrate while the previous formulation allows a contact line to move without slip. Dai et al. [40] signified a problem for the expression derived by Wu and Wang [39], and presented a correction to this formula. This problem refers to the case in which the first and second derivatives of the film are approaching to zero. Biswal et al. [33] included the expression derived by Wu and Wang [39] in the modeling of the evaporation meniscus. They stated that the correction which Dai et al. [40]

applied to the formula is not significantly affecting the result and the expression presented in the study of Wu and Wang, was used as the main formula for calculating disjoining pressure. This study was the only one in which the effect of the slope and curvature dependent disjoining pressure on the evaporation was taken into consideration. There has not been any research related to analyzing the effect of disjoining pressure for condensation film, with or without the slope dependency, up to present day.

CHAPTER 3

MODELING AND SOLUTION METHODOLOGY

3.1 Problem definition

Evaporation mostly occurs in the groove and close to fin edge. The surface on the fin top is assumed to be adiabatic which means no evaporation take places on that surface. Despite the evaporation section, fin top is the most important part of condensation modeling since almost all of the condensation occurs on the fin top due to the thinner liquid film on it in contrast to the liquid inside the groove. The adiabatic transitioning region between condensation and evaporation zone is the section in which any phase change process is neglected in the modeling of heat pipe. The process of phase changes on the fin top and in the grooves along with liquid flow inside the groove is shown in Fig. 3.1. The liquid film is flatter in the ending zone of condensation section and by approaching to the starting point of condensation section, the shape of the liquid film on the fin top and in the groove becomes more curvy. The liquids flows from condensation to evaporation section through the groove because of the pressure gradient created by capillary pressure. In the evaporation section liquid film inside the groove becomes curvy due to evaporation by approaching to the ending zone of this section. In this study, the modeling of condensation film and predictions for its profile is concentrated to the fin top only, since the most margin of condensation is happening on the fin top. The modeling process includes conservation of mass, momentum and augmented Young-Laplace equation in the vapor-liquid interface. In this chapter the modeling process along with the numerical approaches for solving the problem is discussed and presented.

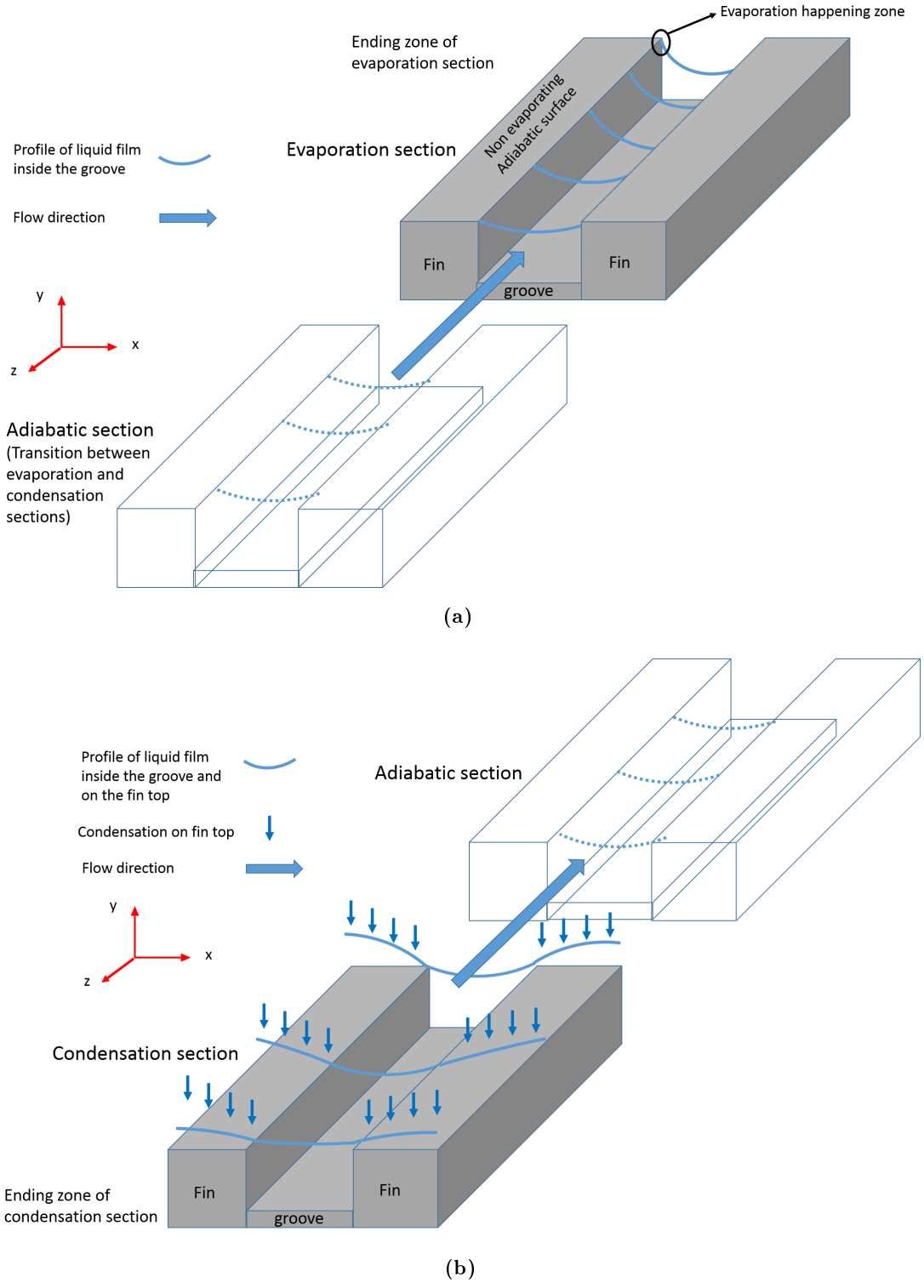

Figure 3.1: (a) Heat pipe mechanism in groove for evaporation and adiabatic sections (b) Heat pipe mechanism in the groove and on the fin top for condensation and adiabatic sections

3.2 Flow and condensation model

Since the film thickness created because of the condensation on the fin top is thinner than the liquid inside the groove, most of the heat transfer process happens on the fin top. Consequently, in order to have a better thermal predictions, an accurate modeling for the condensation film on the fin top is necessary. This liquid film on the fin top and the general geometry of the fin and grooved is shown in Fig. (3.2). The angle α is the contact angle inside the groove and slope of the liquid–vapor interface can be expressed as a function of the angle θ_e, $\delta_x = \tan(\theta_e)$, where the angle θ_e is defined as the "edge slope angle" in the current study. Augmented Young-Laplace equation (Eq. (3.1)) is used for describing the pressure difference between vapor and liquid on the fin top which includes capillary and disjoining pressure terms.

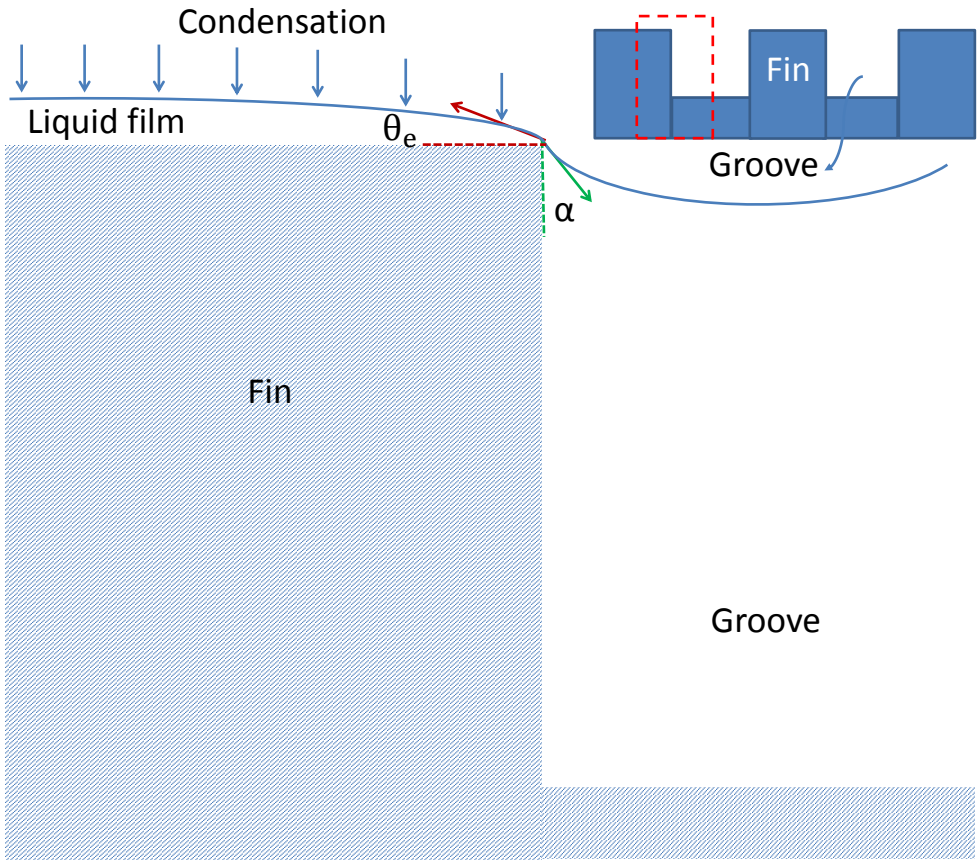

Figure 3.2: Liquid film geometry on the fin top

$$P_v - P_l = P_c + P_d \tag{3.1}$$

The liquid flow on the fin top is assumed as unidirectional fully developed. Inertia terms are neglected and the momentum conservation on the fin top is written as

$$\frac{dP_l}{dx} = \mu \frac{d^2u}{dy^2}. \tag{3.2}$$

In this equation u is the fluid velocity in the streamwise (i.e. x) direction and μ is the dynamic viscosity of the fluid. Integrating Eq. (3.2) along with the boundary conditions $u = 0$ at $y = 0$, and $du/dy = 0$ at $y = \delta$ the velocity distribution is obtained.

$$u(y) = \frac{1}{2\mu} \frac{dP_l}{dx}\, y(y - 2\delta), \tag{3.3}$$

the integration of which gives the mass flow rate per unit depth

$$\dot{m}' = -\frac{1}{3\nu} \frac{dP_l}{dx}\, \delta^3. \tag{3.4}$$

Mass flux at the interfacial region beween vapor and liquid is predicted by using the modified form of the Wayner's equation which was introduced by Moosman and Homsy [41]. This equation is a function of temperature difference between vapor and wall. Pressure difference between the liquid and vapor phases is taken into consideration in this formula.

$$\dot{m}_c'' = \frac{a\,(T_w - T_v) - b\,(P_v - P_l)}{1 + a\delta h_{lv}/k_l} \tag{3.5}$$

$$a = \frac{2c}{2 - c}\Big(\frac{M}{2\pi R_u T_{lv}}\Big)^{1/2} \frac{P_v M h_{lv}}{R_u T_v T_{lv}} \tag{3.6}$$

$$b = \frac{2c}{2 - c}\Big(\frac{M}{2\pi R_u T_{lv}}\Big)^{1/2} \frac{P_v V_l}{R_u T_{lv}} \tag{3.7}$$

The accommodation coefficient, c, is taken as unity in Eq. (3.6,3.7)[13, 18–20, 30, 32]. By applying the mass balance between mass fluxes which are introduced

in Eq. (3.4) and Eq. (3.5), the governing equation which is a function of the film profile, is obtained as

$$\frac{d\dot{m}'}{dx} = -\dot{m}_c''. \tag{3.8}$$

Substitution of the Eq. (3.5) and Eq. (3.4) into Eq. (3.8) results in the governing differential equation for the film thickness, δ in terms of pressures

$$-\frac{1}{3\nu}\delta^3\frac{d^2P_l}{dx^2} - \frac{\delta^2}{\nu}\frac{d\delta}{dx}\frac{dP_l}{dx} = -\frac{a\left(T_w - T_v\right) - b\left(P_v - P_l\right)}{1 + a\delta h_{lv}/k_l}. \tag{3.9}$$

3.3 Capillary and disjoining pressures

Capillary pressure formula which totally dependents on the shape and curvature of the liquid is expressed as,

$$P_c = \frac{\sigma\delta_{xx}}{\left(1 + {\delta_x}^2\right)^{3/2}}. \tag{3.10}$$

The expression for disjoining pressure was introduced by Derjaguin [11] as

$$P_d = \frac{A}{\delta^3}. \tag{3.11}$$

Since this equation is solely function of the film thickness, its best predictions are for parallel surfaces without any slope an curvature for the liquid film. In this study this form of the disjoinig pressure is named as "simple form", where A represent the dispersion constant. In the current study the effect of the slope and curvature of the fluid surface on the disjoining pressure is included. In order to derive the functional form of the disjoinig pressure, the approach that Wu and Wang [39] followed in the derivation of disjoining pressure is used. They derived an expression for the disjoining pressure as Eq. (3.12), yet it should be noted that this expression is only valid for small values of the slope of film thickness.

$$P_d = \frac{B}{\delta^3}\Big(\alpha^4 - {\delta_x}^4 + \delta{\delta_x}^2\delta_{xx}\Big). \tag{3.12}$$

In this equation α and B are constants wrriten in Eq. 3.22. In the condesation region and on the fin top, the liquid film could have slop and curvy shapes, rendering the expression of the disjoning pressure to include higher order terms. As a consequence, a formula including these cited terms is needed. To this end, the same mathematical approach of Wu and Wang [39] is used, but modifications are applied.

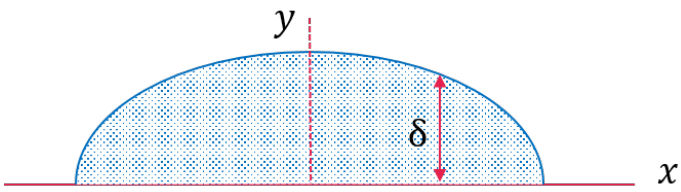

Figure 3.3: A drop on a solid substrate.

Equilibrium condition in which the total energy of the system is at its minimum value and its variation is equal to zero, is written as

$$\bar{\delta}I = 0; \qquad I = \int_0^{x^*} \big(\sigma_{fg}(1+\delta_x)^{1/2} + \sigma_{fs} - \sigma_{sg} + E + L_g\delta\big)dx. \tag{3.13}$$

Expanding Eq. (3.13) gives

$$\int_0^{x^*} \Big(\frac{\partial E}{\partial \delta} + p_c\Big)\omega\delta\, dx + \int_0^{x^*} \Big(\frac{\partial E}{\partial \delta} + \frac{\sigma_{fg}\delta_x}{\big(1+{\delta_x}^2\big)^{1/2}}\Big)\omega\delta_x\, dx + \Big[\sigma_{fg}\big(1+{\delta_x}^2\big)^{1/2} + \sigma_{fs} - \sigma_{sg} + E + p_c\delta\Big]_{x^*}\omega x^* = 0. \tag{3.14}$$

By using integration of parts method for second term and combining the first and second parts, the final expansion of the Eq. (3.13) could be shown as

$$\int_0^{x^*} \left(\frac{\partial E}{\partial \delta} + p_c - \frac{\sigma_{fg}\delta_{xx}}{\left(1+{\delta_x}^2\right)^{3/2}} - \frac{d}{dx}\Big(\frac{\partial E}{\partial \delta_x}\Big) \right) \omega\delta \, dx$$
$$- \left[\Big(\frac{\sigma_{fg}\delta_x}{\left(1+{\delta_x}^2\right)^{1/2}} + \frac{\partial E}{\partial \delta_x} \Big) \omega\delta \right]_{x=0}$$
$$+ \left[\frac{\sigma_{fg}}{\left(1+{\delta_x}^2\right)^{1/2}} + \sigma_{fs} - \sigma_{sg} + E + \delta_x \frac{\partial E}{\partial \delta_x} \right]_{x=x_0} \omega x^* = 0. \quad (3.15)$$

Because $\omega\delta$ and ωx^* are arbitrary, the expressions inside the parentheses and brackets should be equal to zero. The first expression gives the augmented Young-Laplace equation as below,

$$\frac{\sigma_{fg}\delta_{xx}}{\left(1+\delta_x\right)^{3/2}} - \frac{\partial E}{\partial \delta} + \frac{d}{dx}\Big(\frac{\partial E}{\partial \delta_x}\Big) = L_c. \quad (3.16)$$

The first term of Eq. (3.16) expresses the capillary pressure and the term L_c is recognized to be the difference of the vapor and liquid pressure. Consequently, disjoining pressure could be defined as

$$P_d = -\frac{\partial E}{\partial \delta} + \frac{d}{dx}\Big(\frac{\partial E}{\partial \delta_x}\Big). \quad (3.17)$$

Excess energy was derived by integrating the total intermolecular potential Φ with respect to x, from cut-off distance D to the film thickness δ at any given point. This limiting distance D is assigned in order to avoid the infinite self interactions. [39]

$$E = \int_D^{\delta} (\Phi - \Phi_\infty) dy \quad (3.18)$$

Φ and Φ_∞ were found by considering a geometry of a droplet on the substrate and assuming two points, one inside the liquid and the other outside, located in the solid or vapor as shown in Fig. 3.4. Φ is derived by Wu and Wang [39] as

$$\Phi = \frac{\pi n_f^2 \beta_{ff}}{6} \left[\frac{a_1(1-\rho) + \rho - \lambda}{\upsilon_1^3} + \frac{a_2(1-\rho)}{\upsilon_2^3} \right] \quad (3.19)$$

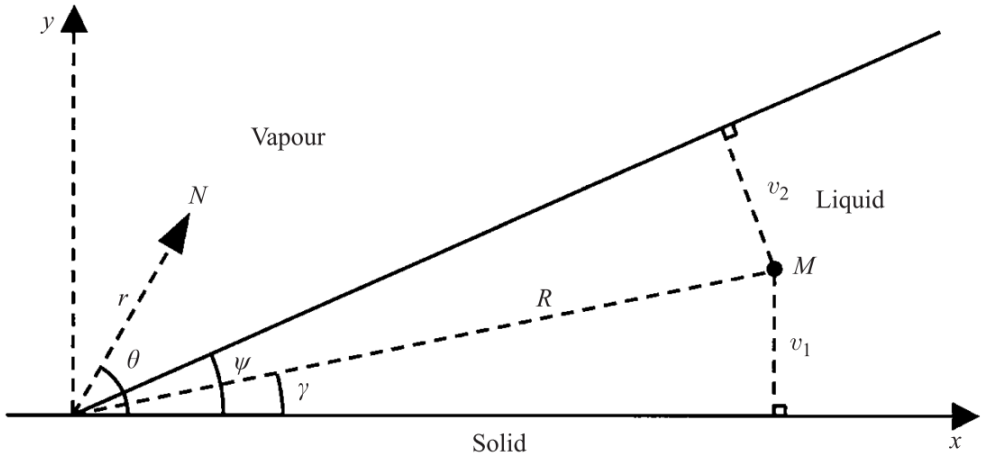

Figure 3.4: A liquid wedge on a solid substrate in equilibrium with its vapor [39]

where,

$$\lambda = \frac{n_s \beta_{fs}}{n_f \beta_{ff}}, \quad \rho = \frac{n_g \beta_{fg}}{n_f \beta_{ff}}, \quad \upsilon_1 = R\ \sin\gamma, \quad \upsilon_2 = R\ \sin(\psi - \gamma)$$

$$a_1 = 1/2 + 3/4\ \cos\gamma - 1/4\ \cos^3\gamma,$$

$$a_2 = 1/2 + 3/4\ \cos(\psi - \gamma) - 1/4\ \cos^3(\psi - \gamma).$$

As υ_1 tends to infinity but making υ_2 to be constant, Φ_∞ could be expressed as

$$\Phi_\infty = \frac{\pi n_f^2 \beta_{ff}(1-\rho)}{6\upsilon_2^3} \tag{3.20}$$

Wu and Wang [39] derived the excess energy as Eq. (3.21), by calculating the van der Waals forces between solid, liquid and vapor molecules and defining the intermolecular distance based on the cylindrical geometry. In order to reach the final format of E, the limit of the Eq. (3.21) for the case that D/δ is approaching to zero should be taken. This assumption is acceptable because of the small ratio of D/δ, otherwise the scale of δ would be small enough to pass the limits of continuum postulate.

$$E = -\frac{\pi {n_f}^2 \beta_{ff}}{4\delta^2}\left(\frac{1-\lambda}{3} + \frac{(1-\rho)\,{\delta_x}^2}{4}\left(1 - \frac{1}{(1+{\delta_x}^2)^{1/2}}\right)\right). \tag{3.21}$$

Disjoining pressure which is expressed as Eq. (3.12) is derived by taking the limit of $\delta_x \to 0$ in Eq. (3.21) and inputting the modified E into Eq. (3.17), but

in this study the excess energy is added to the Eq. (3.17) with the exact form of the Eq. (3.21). Hence, a new form of disjoining pressure, which is compatible for higher rates of slope and curvature, could be defined as

$$P_d = \pm\frac{B}{\delta^3}\Bigg(\alpha^4 - \frac{2}{3}{\delta_x}^2 - \frac{2{\delta_x}^4}{3\left(1+{\delta_x}^2\right)^{3/2}} + \frac{2{\delta_x}^2}{3\left(1+{\delta_x}^2\right)^{1/2}} + \frac{2}{3}\delta\delta_{xx} - \frac{\delta\delta_x{}^4\delta_{xx}}{(1+{\delta_x}^2)^{5/2}} + \frac{5\delta\delta_x{}^2\delta_{xx}}{3\left(1+{\delta_x}^2\right)^{3/2}} - \frac{2\delta\delta_{xx}}{3\left(1+{\delta_x}^2\right)^{1/2}}\Bigg), \quad (3.22)$$

where,

$$B = \frac{3\pi {n_f}^2\beta_{ff}\,(1-\rho)}{16}, \quad \alpha = \left[\frac{8\,(1-\lambda)}{9\,(1-\rho)}\right]^{1/4}, \quad \lambda = \frac{n_s\beta_{fs}}{n_f\beta_{ff}}, \quad \rho = \frac{n_g\beta_{fg}}{n_f\beta_{ff}}.$$

This derived version of the disjoinig pressure is named as "full form" in this study. Using Eq.(3.1) and assuming a constant pressure P_v of vapor phase, and using Eq. (3.10) the pressure gradient in the liquid is found as

$$\frac{dP_l}{dx} = -\frac{d(P_c+P_d)}{dx} = -\frac{dP_d}{dx} - \sigma\frac{\delta_{xxx}}{(1+{\delta_x}^2)^{3/2}} + 3\sigma\frac{\delta_x\delta_{xx}}{(1+{\delta_x}^2)^{5/2}}. \quad (3.23)$$

This new form of disjoining pressure was added to Equations. (3.23) and (3.9) which results in a 4^{th} order nonlinear ordinary differential equation as a final governing equation. In summary, the general differential equation of the problem for a case in which disjoning pressure is excluded and included, are defined as Equations 3.24 and 3.25. Governing equation for the case in which the disjoning pressure is not included in the modeling is

$$\frac{1}{3\nu}\frac{d}{dx}\left[\delta^3\frac{d}{dx}\Big[\frac{\sigma\delta_{xx}}{\left(1+{\delta_x}^2\right)^{3/2}}\Big]\right] = -\frac{a\,(T_w-T_v) - b(\sigma\delta_{xx}/(1+{\delta_x}^2)^{3/2})}{1+a\delta h_{lv}/k_l}. \quad (3.24)$$

By adding Eq. 3.22 to Eq. 3.9, governing equation which includes the full form

of the disjoning pressure could be defined as

$$\frac{1}{3\nu}\frac{d}{dx}\Big[\delta^3\frac{d}{dx}\Big(\pm\frac{B}{\delta^3}\big(\alpha^4-\frac{2}{3}{\delta_x}^2-\frac{2{\delta_x}^4}{3\left(1+{\delta_x}^2\right)^{3/2}}+\frac{2{\delta_x}^2}{3\left(1+{\delta_x}^2\right)^{1/2}}+\frac{2}{3}\delta\delta_{xx}$$
$$-\frac{\delta{\delta_x}^4\delta_{xx}}{(1+{\delta_x}^2)^{5/2}}+\frac{5\delta{\delta_x}^2\delta_{xx}}{3\left(1+{\delta_x}^2\right)^{3/2}}-\frac{2\delta\delta_{xx}}{3\left(1+{\delta_x}^2\right)^{1/2}}\big)+\frac{\sigma\delta_{xx}}{\left(1+{\delta_x}^2\right)^{3/2}}\Big)\Big]=$$
$$-\frac{1}{1+a\delta h_{lv}/k_l}\Big[a\left(T_w-T_v\right)-b\Big(\pm\frac{B}{\delta^3}\big(\alpha^4-\frac{2}{3}{\delta_x}^2-\frac{2{\delta_x}^4}{3\left(1+{\delta_x}^2\right)^{3/2}}+\frac{2{\delta_x}^2}{3\left(1+{\delta_x}^2\right)^{1/2}}$$
$$+\frac{2}{3}\delta\delta_{xx}-\frac{\delta{\delta_x}^4\delta_{xx}}{(1+{\delta_x}^2)^{5/2}}+\frac{5\delta{\delta_x}^2\delta_{xx}}{3\left(1+{\delta_x}^2\right)^{3/2}}-\frac{2\delta\delta_{xx}}{3\left(1+{\delta_x}^2\right)^{1/2}}\big)+\frac{\sigma\delta_{xx}}{\left(1+{\delta_x}^2\right)^{3/2}}\Big)\Big]. \tag{3.25}$$

It is obvious that including the effect of disjoning pressure makes the governing equation to be highly nonlinear, which should carefully be addressed by numerical approaches with suitable accuracy in order to find the accurate roots.

3.4 Solution methodology

In this section the boundary conditions for the problem are defined. Numerical solution of two methods for the problem are introduced and finally the flowcharts of the numerical processes are presented.

3.4.1 Boundary and initial conditions

Boundary conditions are chosen based on the physics of the problem. As it is shown in the Fig. (3.2), four boundary conditions are available for the flow on the fin top. Two of them are defined at the symmetry line and the other two are located at the edge of the fin. First derivative of the film thickness is defined in relation with complementary angle at the fin edge by $\delta_x(L) = -\tan\theta_c$. In order to satisfy the concavity change of the film profile on the fin top and in the groove, the second derivative of the film thickness should be considered to be zero at the fin edge. The first derivative of the film is set be zero in order to impose the symmetric condition to the film profile at the centerline. Fourth boundary condition refers to the third derivative, which is assumed to be zero

at the center line. This consideration satisfies two different demands; (i) it guarantees the symmetric condition for the film thickness, (ii) it could avoid any unintended entrance of mass flow rate at the centerline. If we divide the fluid film into several infinitesimal elements and consider the first element at the beginning, due to the mass balance there should not be any $m^{'}_{in}$ for the first element. In order to make sure that $m^{'}_{in}$ is equal to zero, it could be understood from Eq. (3.4) that the pressure gradient should be imposed to be zero. Pressure gradient is both function of first and third derivatives, as a result, enforcing first derivative to be zero could not make $m^{'}_{in}$ to be zero because of the presence of the terms which are solely function of the third derivative in pressure gradient. By considering both derivatives to be zero, it could satisfy the symmetric condition and avoid the possible mass entrance at the centerline simultaneously.

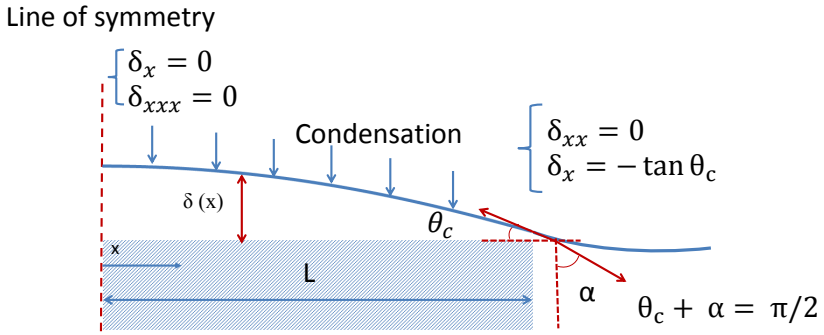

Figure 3.5: Boundary and matching conditions frequently used in the literature

In summary the boundary conditions are,

$$\text{At } x = 0: \quad \delta_x = 0, \quad \delta_{xxx} = 0;$$

$$\text{At } x = L: \quad \delta_x = -\tan\theta_c, \quad \delta_{xx} = 0. \quad (3.26)$$

An alternative set of boundary conditions are used in order to investigate the validity and applicability of the matching condition at the fin edge. In this case, the location in which the second derivative of the profile change its sign is set to be in a spot before the fin edge, as observed experimentally [5]. This second set of boundary conditions is shown in in Fig. 3.5.

$$\text{At } x = 0: \quad \delta_x = 0, \quad \delta_{xxx} = 0;$$
$$\text{at } x = x_i: \quad \delta_{xx} = 0$$
$$\text{at } x = L: \quad \delta_x = -\tan\theta_e, \ \theta_e = 0 \quad (3.27)$$

The schematic of this set of boundary conditions is plotted in Fig. 3.6.

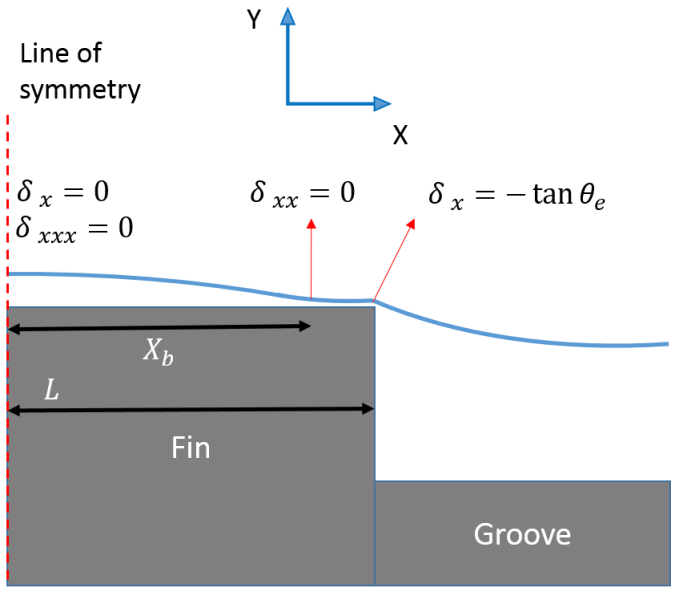

Figure 3.6: Alternative set of Boundary and matching conditions, adaptation by experimental data [5]

3.4.2 Numerical approaches

The governing equation of the condensation film was solved numerically in two different ways. The first method is based on using Runge-Kutta-Fehlberg approach for solving the 4th order nonlinear differential equation. The second one which is commonly used in literature, is to fit a 4^{th}order polynomial to the governing equation. Both of the mentioned solution methods are used and modeled in this study. In this section solution procedures of these two cited approaches are discussed and explained.

3.4.2.1 Secant method for 4thorder polynomial model

4thorder polynomial integration method was used in this study, in which the same methodology is applied as the one was introduced by Do et al. [20, 24]. In this approach, a 4th order polynomial is assumed as a function of film thickness and its constants are defined by considering the boundary conditions. This polynomial could be written as

$$\delta = \alpha_0 + \alpha_1 (x - t) + \alpha_2 (x - t)^2 + \alpha_3 (x - t)^3 + \alpha_4 (x - t)^4. \tag{3.28}$$

Where t represent the fin length at the fin edge. α_1, α_2, α_3 and α_4 could be identified by applying the boundary conditions to the Eq. (3.28), but α_0 which is the amount of δ_{edge}, should be assumed as an initial guess. This initial guess is changing by iterative process unless Eq. (3.29) is satisfied, where f is a small parameter chosen dependent on the numerical criteria.

$$-\frac{1}{3\upsilon}\frac{dP_l}{dx}\delta^3 + \int_0^t \frac{a\,(T_w - T_v) - b\,(P_c + P_d)}{1 + a\delta h_{lv}/K_l} = f \tag{3.29}$$

Iteration process of Eq. 3.29 is performed by using secant numreical method. This model is defined in Chapter 4 and its results are discussed.

3.4.2.2 Runge-Kutta-Fehlberg for mass conserving model

The governing 4thorder ODE for the film thickness δ (Eq. (3.9)), is written in the standard R-K form as four coupled first order ODE's

$$\frac{d^4\delta}{dx^4} = f\left(\delta, \delta_x, \delta_{xx}, \delta_{xxx}\right), \tag{3.30}$$

$$\frac{d\delta}{dx} = w, \quad \frac{dw}{dx} = q, \quad \frac{dq}{dx} = z, \quad \frac{dz}{dx} = f\left(\delta, w, q, z\right). \tag{3.31}$$

Solving the equation with Runge-Kutta-Fehlberg method needs four initial conditions. It means the two conditions at the fin edge should be replaced with two assumed new conditions at the centerline in this problem. Two initial conditions are guessed at the center line but these guesses should be altered unless the defined two conditions at the fin edge are satisfied. As a result, at the centerline four conditions are applies as below,

$$x = 0 \quad \rightarrow \delta_0 \ = \text{guessed}, \quad \delta_{\text{x}} = 0, \quad \delta_{\text{xx}} = \text{guessed}, \quad \delta_{\text{xxx}} = 0$$

and the δ_0 and δ_{xx} at the centerline are changing continuously unless the two conditions at $x = L$ are satisfied. A two dimensional Newton-Raphson approach is chosen for finding the roots of the shooting method. Variable step size and quadruple precision are adapted to Runge-Kutta-Fehlberg scheme. Since the equation is purely nonlinear, it is strongly sensitive to the initial guesses.

3.4.2.3 Flowcharts of the numerical process

Flowchart of the numerical process for both set of boundary conditions described in Equations (3.26) and (3.27), are presented in Figs. 3.7 and 3.8. The numerical modeling of the problem with boundary conditions of 3.26, contains two external iterative loops for reaching the θ_{final} and ΔT_{final} by starting from initial values and continues by a small step side. These initial values for θ_i and ΔT_j usually are the fastest and simplest θ_c and ΔT that can be achieved by code. Initial guesses for the RKF-45 (Runge-Kutta-Fehlberg) is assumed and the results are obtained. Boundary conditions at the fin edge, are satisfied by two forcing functions and using two dimensional Newton-Raphson method. In the second numerical process in which the second set of boundary conditions 3.8 is used, there is one external iterative loop for finding the X_b. This location is defined in order to find a location in which the sign of second derivative is changing before the fin edge. The film profile is solve by RKF-45 in two separated sections, before and after the X_b. The forcing functions for correcting the initial guesses are the magnitude of the mass flow rate at fin edge and the second derivative at X_b.

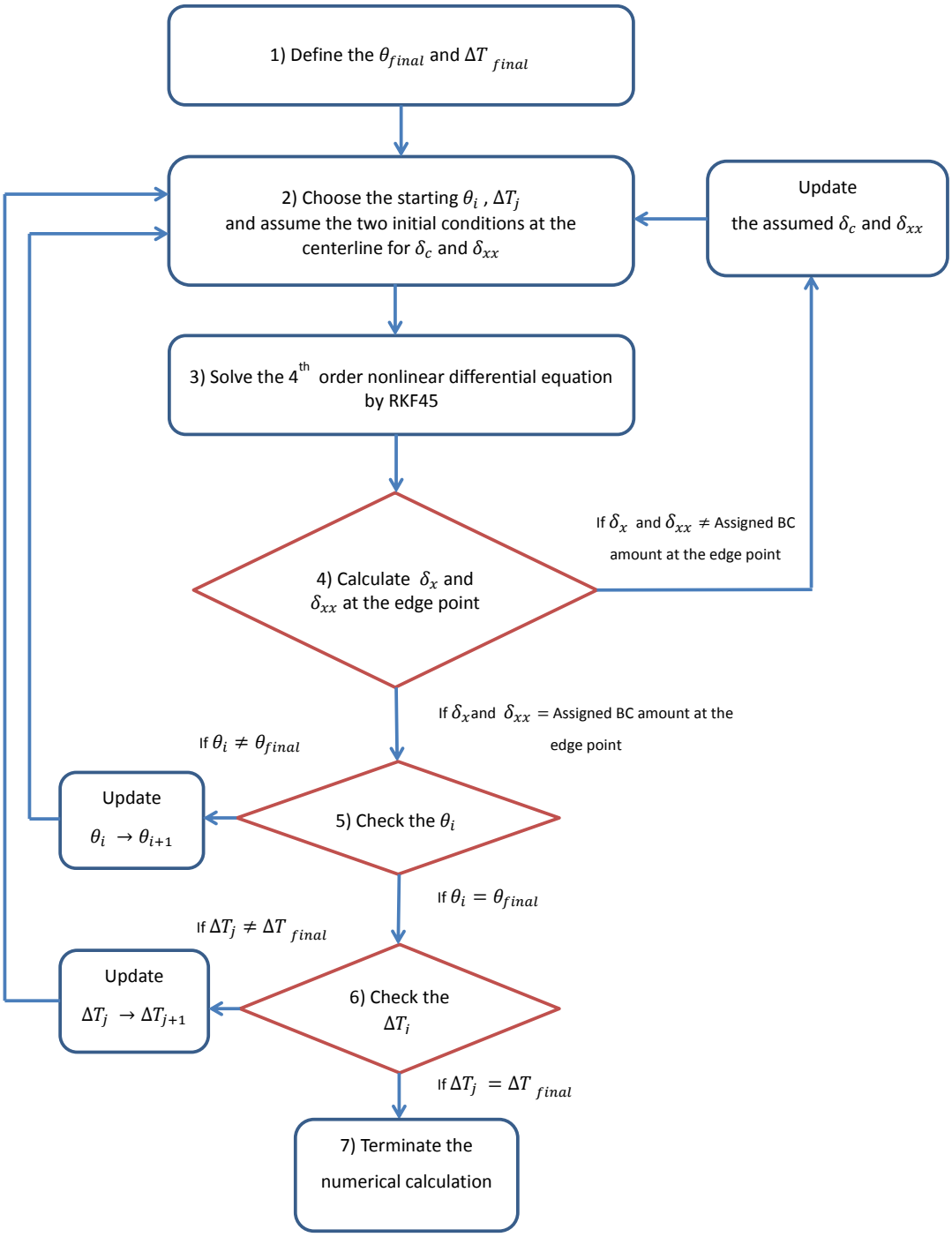

Figure 3.7: Flowchart of the numerical approach

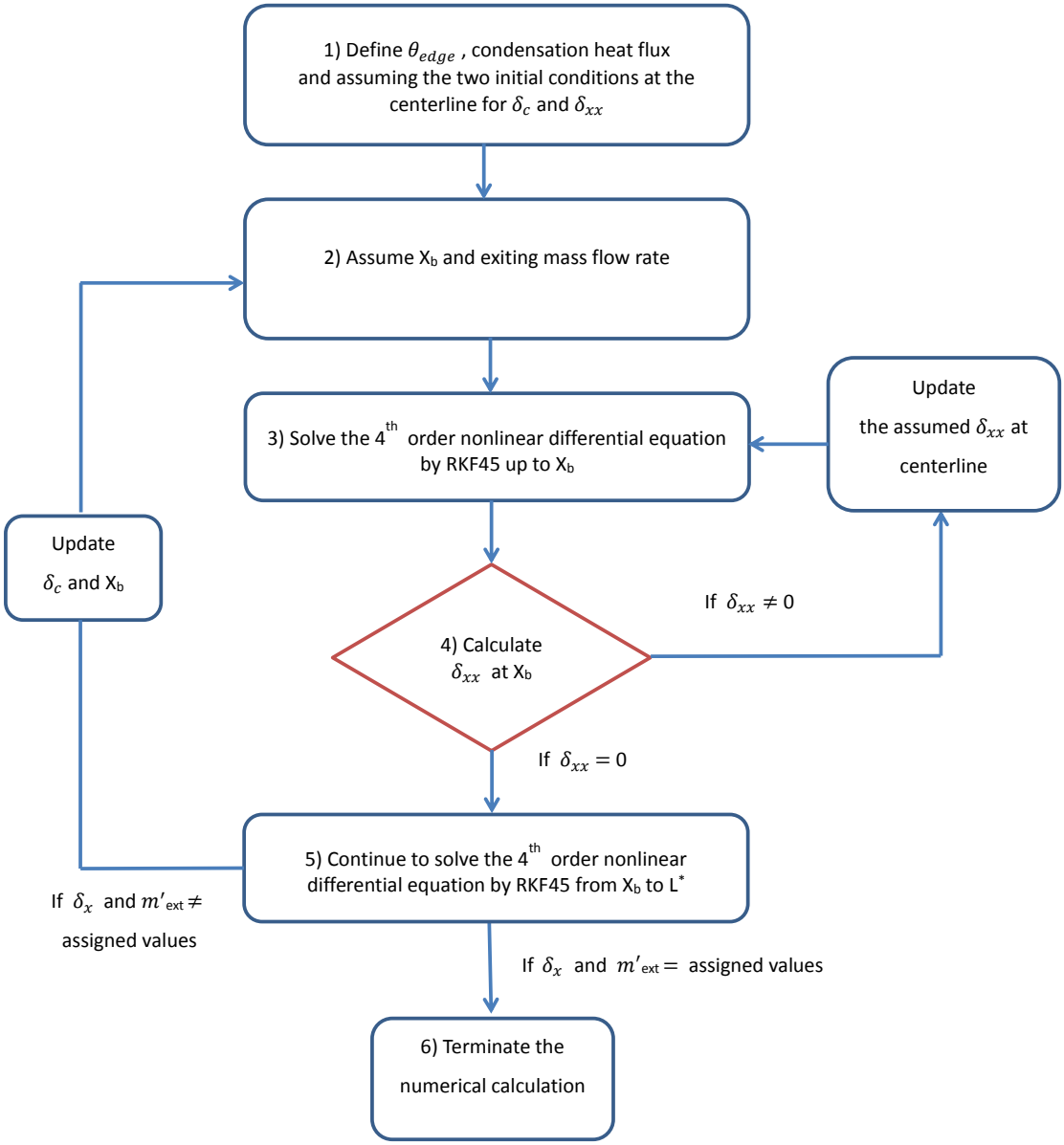

Figure 3.8: Flowchart of the numerical approach for the second set of boundary conditions

CHAPTER 4

NUMERICAL RESULTS AND ANALYSIS

Numerical results are obtained by using numerical approaches stated in section 3.4. The models used in this study are listed as follow:

- 4^{th}order polynomial: Fits a 4^{th}order polynomial to the shape of the liquid film as in [20, 24].

- Young-Laplace (YL): Assumes the pressures to be due to the capillary effect only (P_c), neglecting the disjoining pressure (P_d), and solves the resulting differential equation, Eq. 3.24, for film thickness using Runge-Kutta-Fehlberg approach. This model is mainly constructed in order to analyze and compare the effect of disjoning pressure which is discussed in Section 4.4.

- Augmented Young-Laplace (A-YL): Includes the effect of both capillary (P_c) and disjoining (P_d) pressures. It accounts for the effect of interface slope and curvature on disjoining and capillary pressures, and solves the resulting differential equation, Eq. (3.25), for film thickness using Runge-Kutta-Fehlberg approach.

The problem is formulated for both constant temperature and constant flux boundary conditions. Fin thickness is 20 micron, the operating fluid is water. The physical properties that are used in this study are listed as table. 4.1.

If Eq. (3.22) is used for the parallel surfaces—i.e imposing the first and second derivative to be zero— its format simplifies to a form introduced by Derjaguin [11],

Table 4.1: Physical properties used in condensation modeling

Parameter	Unit	Magnitude
P_v	Pa	1.033×10^5
T_v	K	373
h_{lv}	J/kg	2.3×10^6
ρ	kg/m^3	1000
σ	N/m	5.89×10^{-2}
μ	Pa $\cdot$ s	2.79×10^{-4}
k_l	W/m $\cdot$ K	0.6
M	kg/mol	18×10^{-3}
V_l	m^3/mol	18×10^{-6}
c		1.0
A*		5×10^{-21}

* Taken from[20]

$$P_d = \frac{A}{\delta^3}. \tag{4.1}$$

Comparing Eq. [3.22] and Eq. [4.1], $B\alpha^4 = A$, where A is the dispersion constant. The value of A for water and copper interaction, is obtained from [20] and the value of $B\alpha^4$ is calculated to match A.

4.1 4$^{\text{th}}$order polynomial model

The results of the film profile for 4 different complementary angle with $\Delta T = 1°$C is plotted in Fig. 4.1 for 4$^{\text{th}}$order polynomial model. Forcing the first derivative at the fin edge render the film thickness at the centerline to be completely dependent on this boundary condition. By increasing the magnitude of the complementary angle, the film profile at the centerline becomes thicker despite its manner at the fin edge which reaches thinner thicknesses. Variation of the film thicknesses with temperature difference is presented at Fig. 4.2. By increasing the temperature difference between vapor and wall, the entering condensation

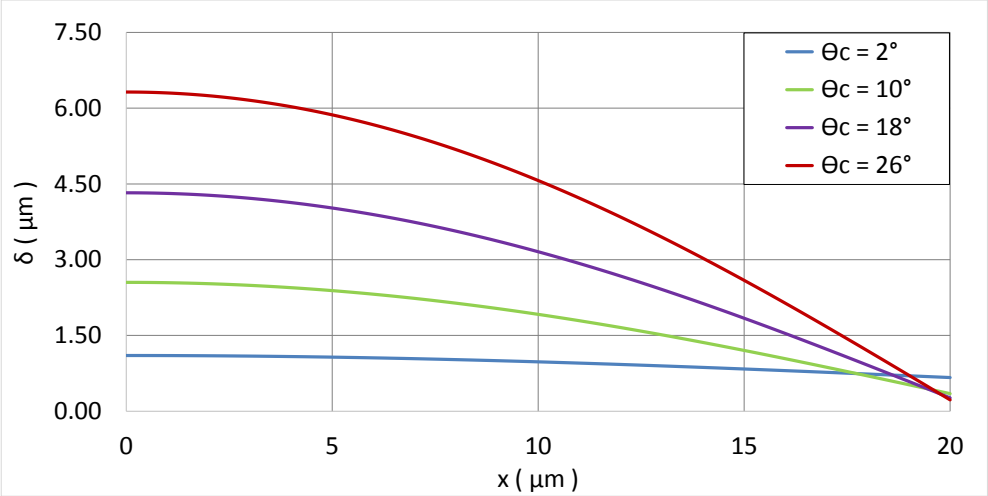

Figure 4.1: Variation of film thickness along the fin for various complementary angles for $\Delta T = 1$ for 4^{th}order polynomial model.

mass flux is increasing and consequently the film becomes more thicker.

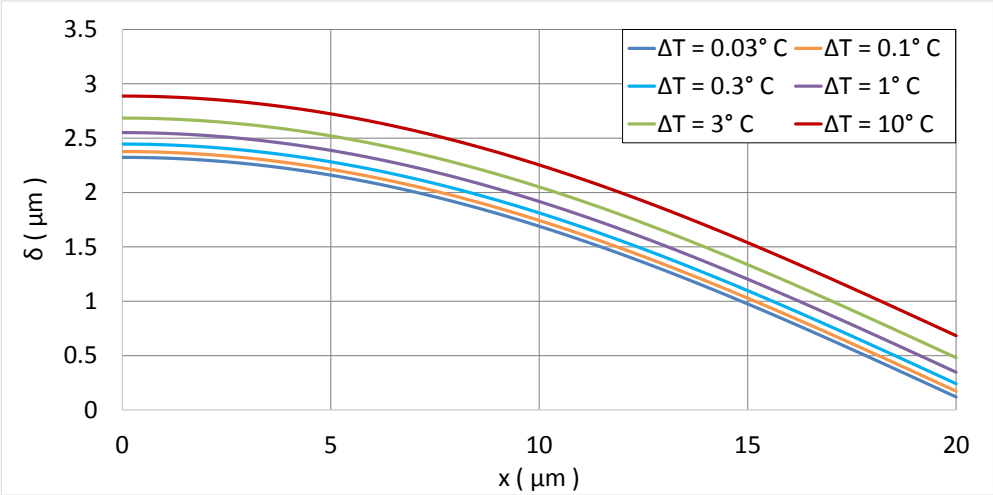

Figure 4.2: Variation of film thickness along the fin for various complementary angles for $\theta_e = 10°$ for 4^{th}order polynomial model.

4.2 Augmented Young-Laplace (A-YL) model

Variation of film profile with respect to different complementary angles and temperature differences for (A-YL) model is presented in Fig. 4.3 and Fig. 4.4. It can be seen from Fig. 4.3 that, same as 4^{th}order polynomial model results, by decreasing the complementary angle the film profile becomes flatter. Fig. 4.4

shows that for smaller temperature differences the film is thinner.

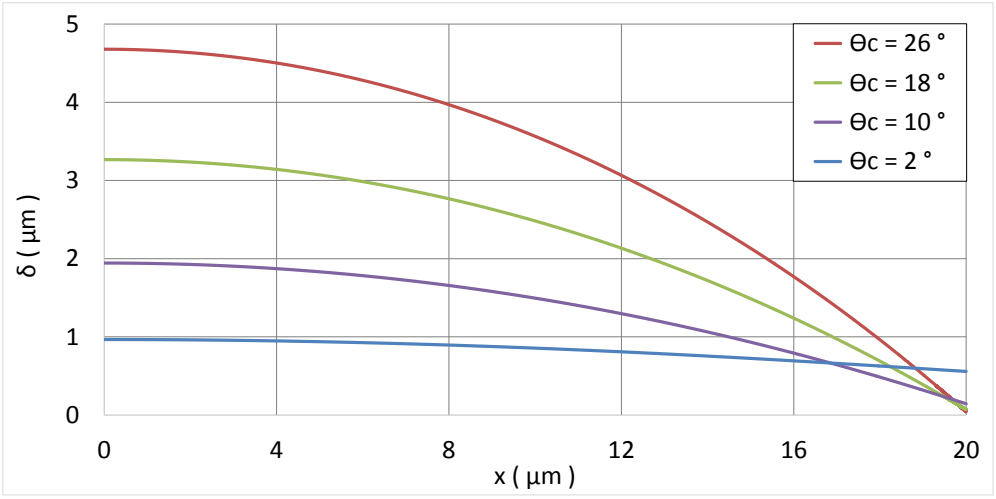

Figure 4.3: Variation of film thickness along the fin for various complementary angles for $\Delta T = 1°C$ (A-YL) model.

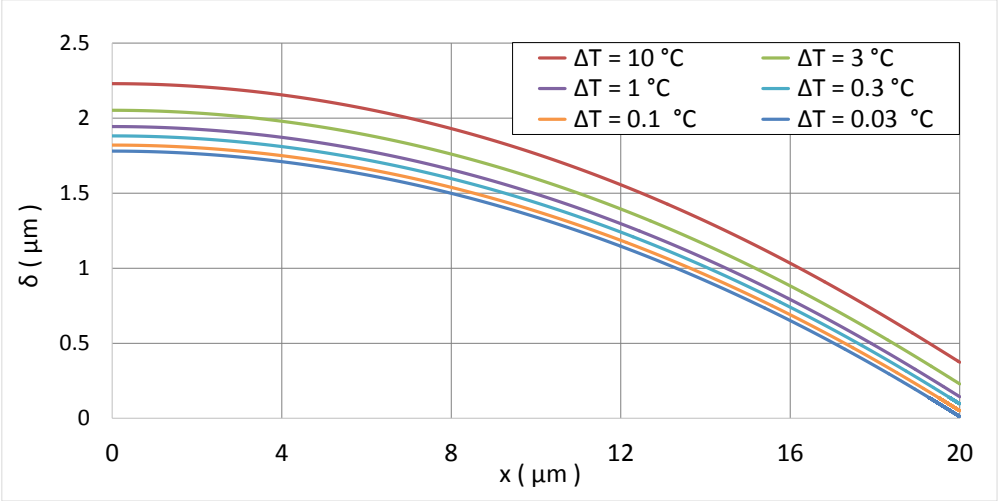

Figure 4.4: Variation of film thickness along the fin for various temperature differences for $\theta_e = 10°$ for (A-YL) model.

The change between the film profiles along the fin and by altering the temperature difference, tends to be almost linear for profiles with thicker thickness. When the film is thick in higher temperature differences, the thickness of the film profile all over the fin top is big enough to neglect the effect of disjoining pressure. By recalling the Eq. 3.5, it can be noted that by increasing the magnitude of the δ, the magnitude of $a(\Delta T)$ becomes dominant in comparison of $b(\Delta P)$ and $ah_{lv}\delta/k_l$, rendering the mass flux to be solely sensitive to ΔT. By

increasing the complementary angle, which means the profile contain more curvy shape and reaches thinner thicknesses at the regions near to fin edge, this mentioned sensitivity to the temperature differences looses its effect. This change is shown in Fig. 4.5 where the film thickness for two different complementary angle but for a same temperature differences is plotted.

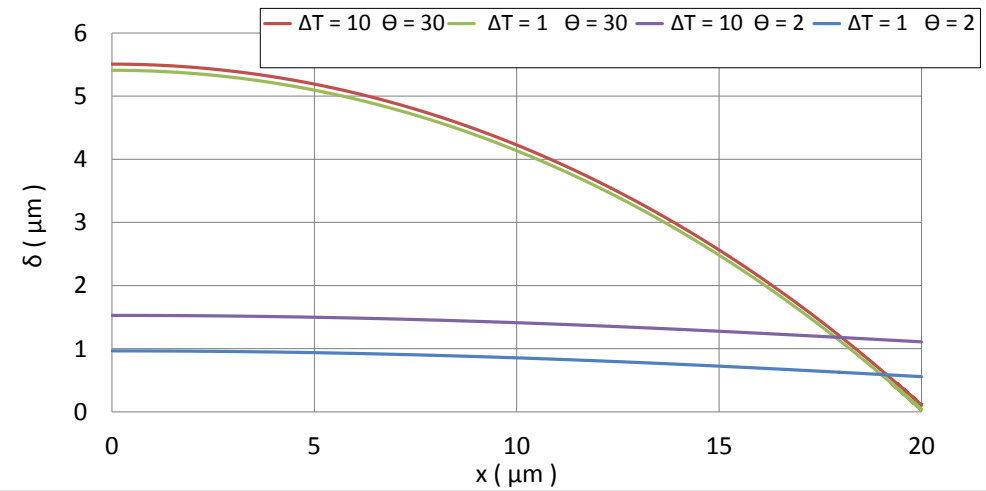

Figure 4.5: Variation of film thickness along the fin for (A-YL) model.

4.3 Validation and comparison

4.3.1 Validation using data available in literature

The results of this study are validated with numerical predictions reported in the literature. The results of the (A-YL) model, 4^{th}order polynomial and the results reported by Faghri and Zhang [4] using VOF method for $\theta_c = 6°$ and $\theta_c = 2°$ at $\Delta T = 10°\text{C}$ are given in Fig. 4.6. The (A-YL) model predicts more condensation since the film thickness is thinner in this case comparing to other models.

Diffrenec between the mass flow rate predictions using (A-YL) model and the 4^{th}order approximation are given in Fig. 4.8. This figure shows a notable difference between the predictions. 4^{th}order profile uses the entire surface of the liquid film for satisfying conservation of mass and momentum, unlike the (A-YL)

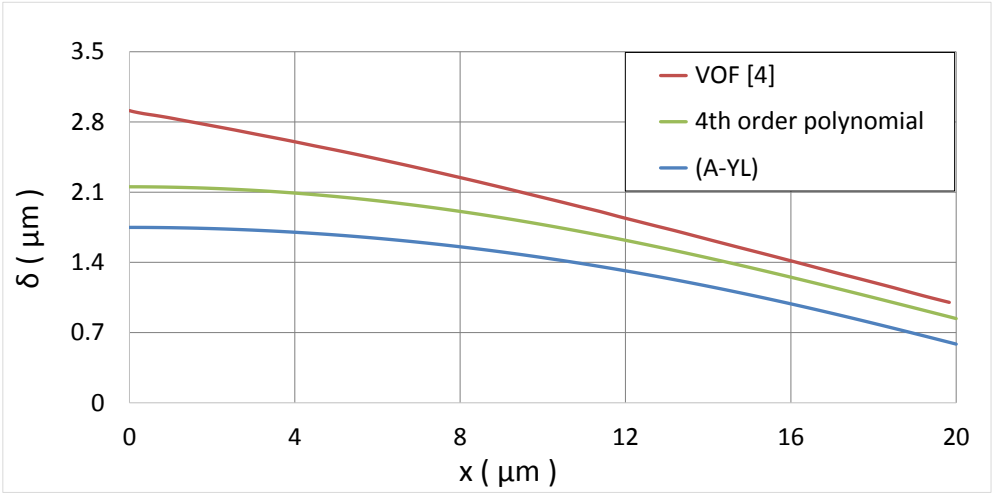

(a) $\theta_e = 6°$

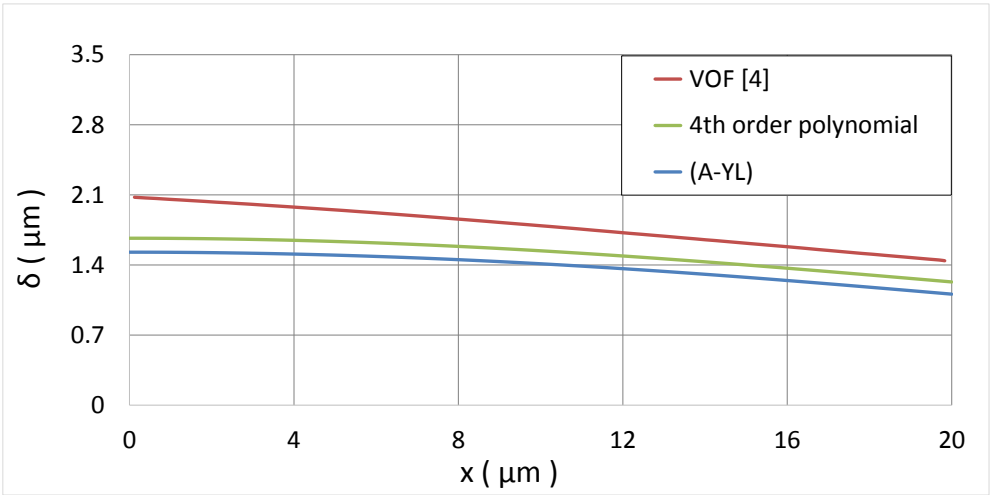

(b) $\theta_e = 2°$

Figure 4.6: Film profile comparison for (A-YL), 4^{th}order polynomial model and VOF method for $\Delta T = 10°\text{C}$

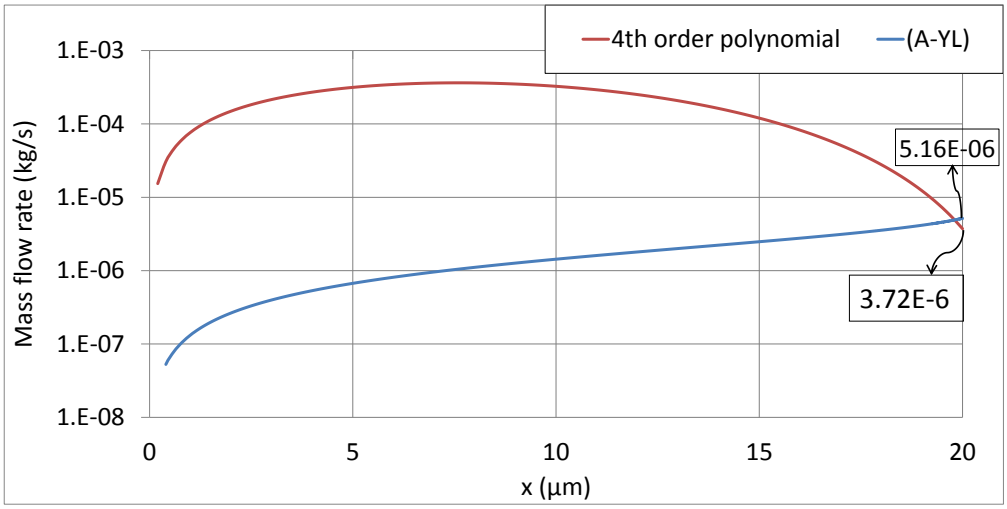

Figure 4.7: 4th order polynomial and (A-YL) model mass flow rate comparision for $\Delta T = 1°C$ and $\theta_e = 10°$

model which uses infinitesimal element for controlling the mass and momentum balance. This difference is visible in Fig. 4.8, which shows that the difference between the results of two methods is less significant when the film profile is flatter. This cited reason could be better shown by plotting the mass flow rate along the fin top for two models with a specific complementary angle in Fig. 4.7. Mass conserving behavior of the (A-YL) model is obvious in this figure, since the magnitude of the mass flow rate is increasing step by step because of the inputting condensation.

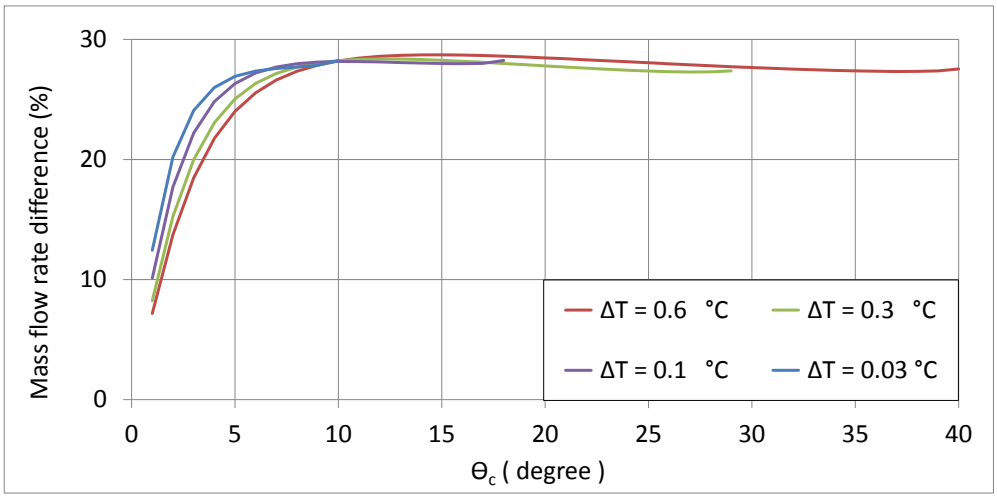

Figure 4.8: Mass flow rate percentage difference for (A-YL) and 4^{th}order polynomial models

In the report that was presented by Lefèvre et al. [5], condensation film was

modeled by assuming the constant heat flux along the fin top and neglecting the disjoning pressure in the modeling process. Wall shear was calculated by considering a laminar flow in the channel and it was predicted by using a correlation which was based on minimum aspect ratio c_{min}. The numerical value of the c_{min} was not reported in the paper. In order to have a comparision, the model used in [5] is constructed and implemented in this study and different minimum aspect ratios are exercised. Predictions of the film thickness reported in [5], and the results that are obtained in this study by using the (YL) and (A-YL) models and construction of the [5] model with using different values of the minimum aspect ratio are presented in Fig. 4.9. The predictions of the current (YL), (A-YL) models and the reconstructed model using a minimum aspect ratio $c_{min} = 1$ match well. The thickness of the liquid film render the dosjoning pressures effect to be substantial small and negligible which makes the predictions of (Y-L) and (A-YL) models to be in strongly similar magnitudes.

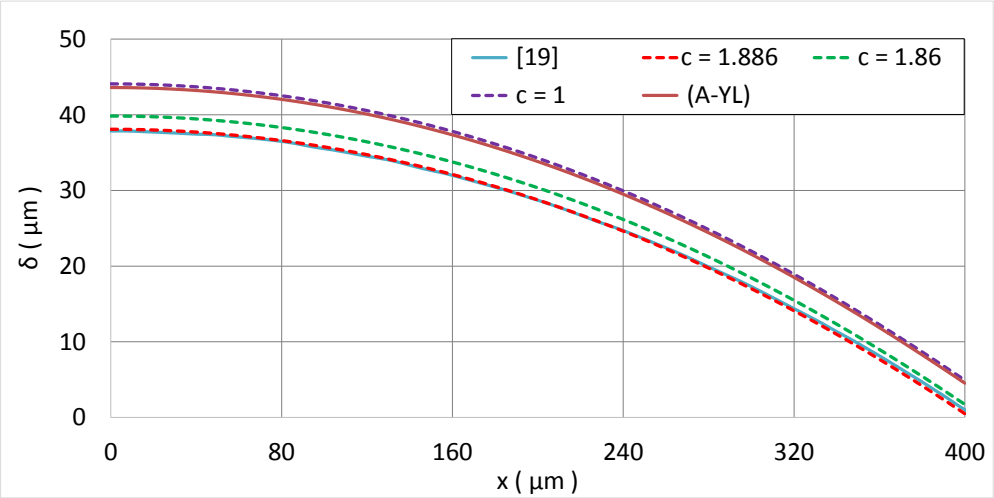

Figure 4.9: Film thickness calculated by (A-YL) model and Lefèvre [5]

4.3.2 Comparison between three models

By plotting the film thickness at the fin edge for all three models introduced at section 4, differences between these mentioned models could be better analyzed. Since film thickness at the edge, (δ_{edge}), is the thinnest thickness of the film profile, the disjoning pressures effect is in its most dominant case along the fin. Consequently, the values of (δ_{edge}) for all three models are plotted. Figs.

4.10 and 4.11 show a notable difference between 4thorder polynomial and (A-Yl) model for (δ_{edge}). The main difference between (A-YL) and (YL) refers to the limitation emerges in (A-YL) results. The reasons rendering this difference is discussed in section 4.4. It should be noted that, this thickness which is predicted for film profile especially at edge zone of the fin top, is calculated by considering the ideal surface for the fin top. Since the scale of the film thickness is less than 1 micron, the surface roughness could readily affects the film shape. In this study the surface is considered to be ideal for all modeling processes.

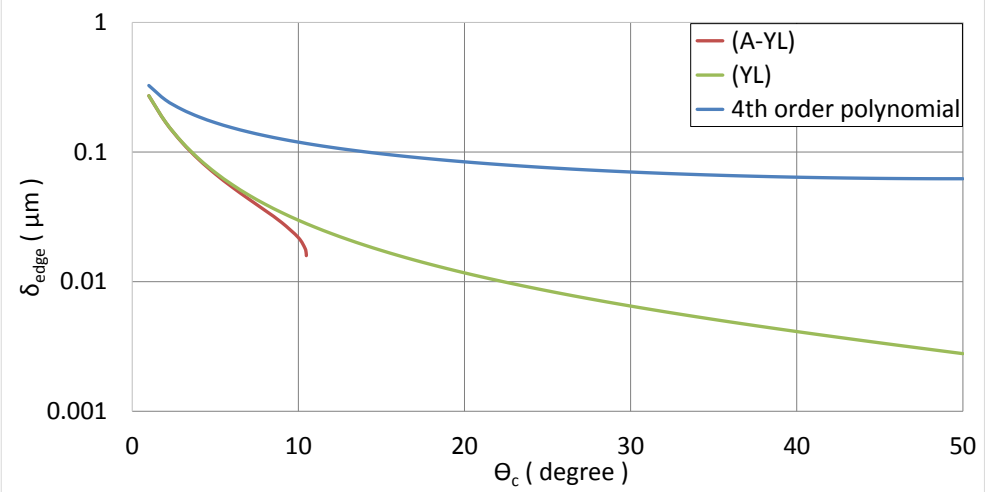

Figure 4.10: δ_{edge} for $\Delta T = 0.03°C$

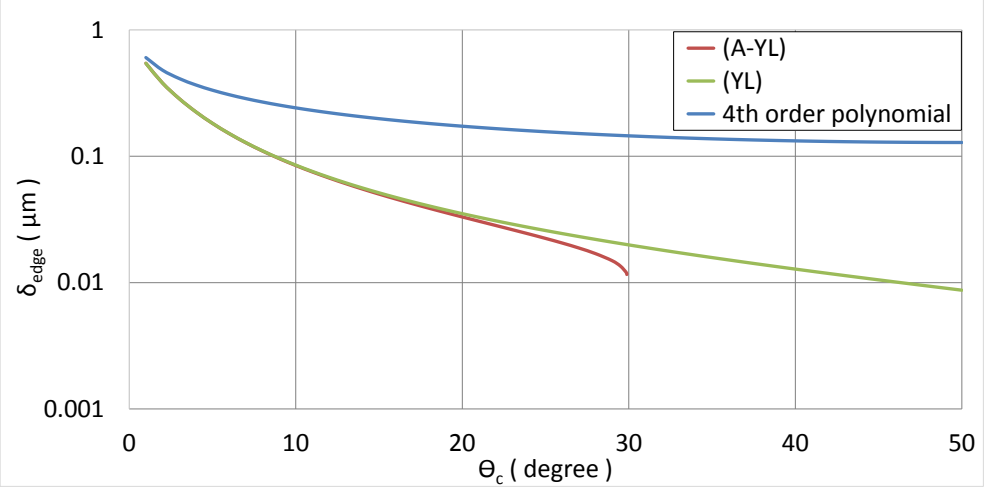

Figure 4.11: δ_{edge} for $\Delta T = 0.3°C$

Predicted mass flow rate difference between (A-YL) and (YL) models is shown in Fig. 4.12. The difference is far lesser than the mass flow rate difference between

4^{th}order polynomial and (A-YL) models. It should be noted that the main notable difference between (A-YL) and (YL) models refers to the existence of a limitation in results of (A-YL) model which is discussed in section 4.4.

Total heat flux analyzing of (A-YL) model, is plotted in Fig. 4.13 with respect to different values of complementary angle and temperature differences. Heat flux is found by multiplying latent heat of evaporation and the total mass flow rate calculated from Eq. 3.4. The magnitude of the heat flux rises by increasing the temperature difference between fin and the interface. By analyzing this figure, it could be understood that heat flux magnitude reaches its maximum value at at a specific complementary angle. There is an extremum point at the beginning of the each profile and this extremum becomes more obvious by increasing the temperature difference. Increasing the number of fins by having thinner width increases the magnitude of the heat fluxes. This suggest that by decreasing the fin thickness, more optimized and enhanced thermal performance is achievable. This effect of fin thickness on the total heat flux is shown in Fig. 4.14 for a range of complementary angles. In order to compare the results of heat fluxes predicted with all three models, Figs. 4.15 and 4.16 are plotted. Like the results of (δ_{edge}), there is a significant difference between the results of 4^{th}order polynomial and (A-YL) models. The result of (A-YL) and (YL) are in good compatibility, the only difference is the existence of limitation for the results of (A-YL) which is explained in section 4.4.

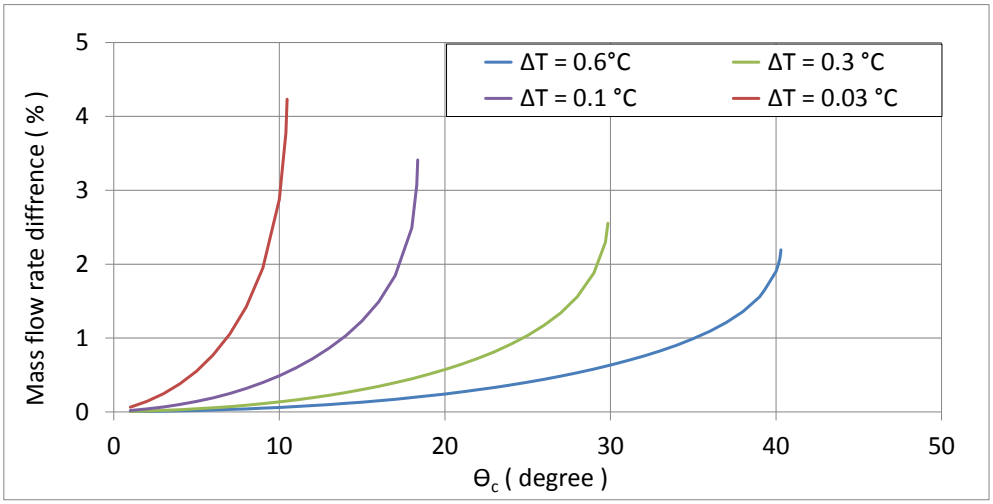

Figure 4.12: Mass flow rate percentage difference for (A-YL) and (YL) models

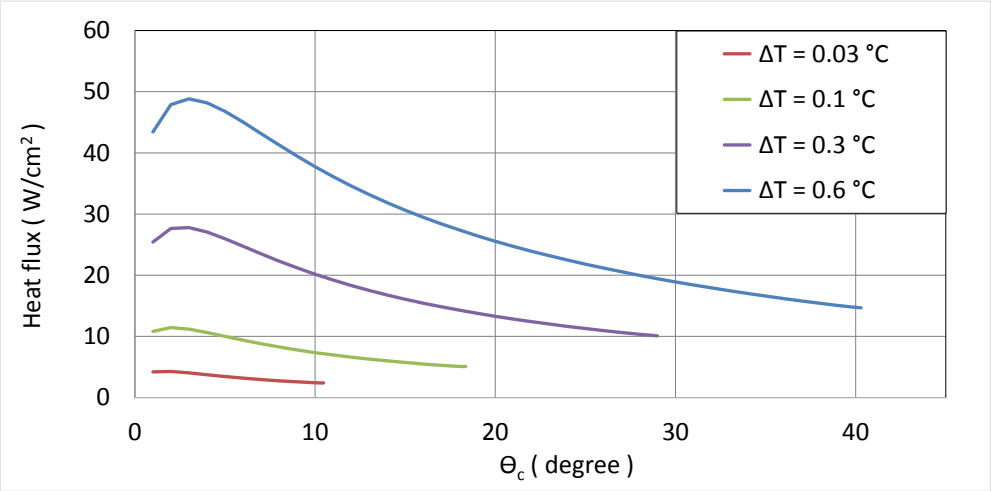

Figure 4.13: Variation of heat flux with complementary angle for (A-YL) model

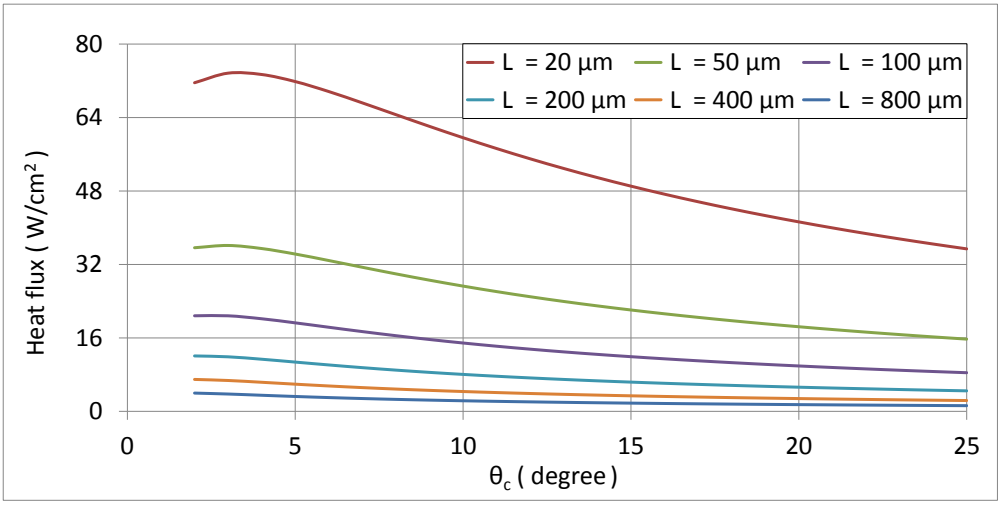

Figure 4.14: Variation of heat flux in (A-YL) model with complementary angle for different fin thicknesses

4.4 Effect of disjoining pressure

In order to analyses the effect of disjoning pressure on the shape of liquid film, the case in which the film is continues at the fine edge is chosen and boundary conditions described in Fig.3.5 are used. In this case edge angle is equal to complementary angle, $\theta_e = \theta_c$. Magnitude of the doisjoning pressure is proportional to the inverse value of the film thickness, which means its effect is dominant when the film thickness is small. Smaller complementary angles, render the liquid film to be flatter which makes the disjoning pressure effects to be distributed on the whole length of the fin but with the smallest magnitude. In contrast, in

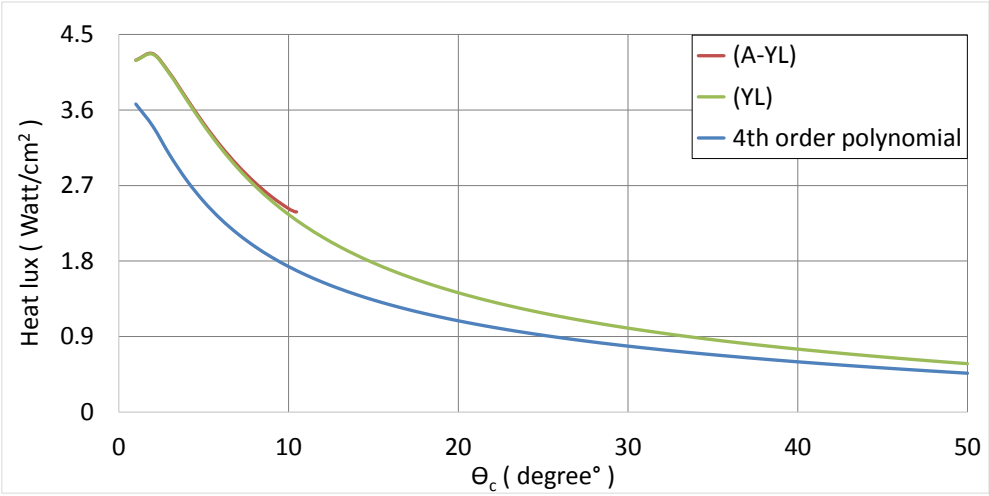

Figure 4.15: Heat flux comparison with different models for $\Delta T = 0.03°C$

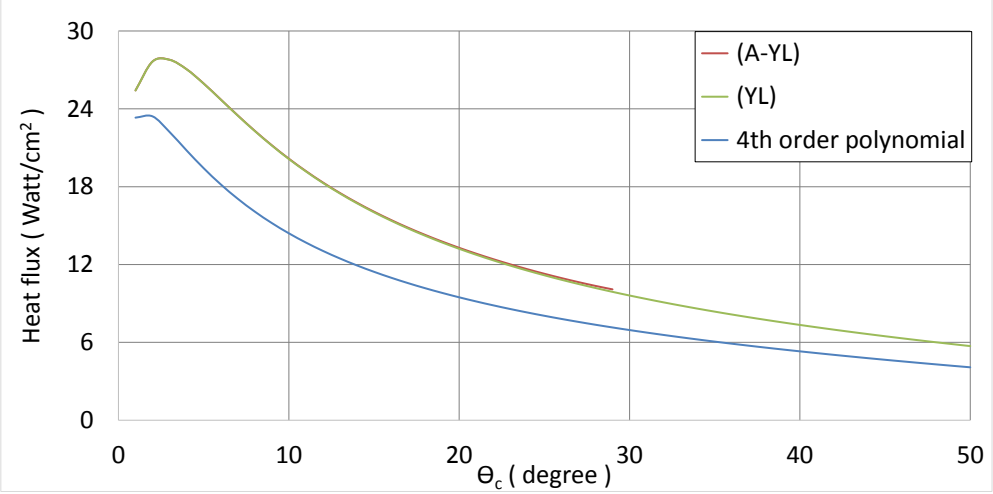

Figure 4.16: Heat flux comparison with different models for $\Delta T = 0.3°C$

higher slopes, film thickness reaches extremely thinner magnitudes at proximity of the fin edge. It means that the effect of disjoning pressure becomes dominant at that small zone before the fin edge. Generally, its effect is more dominant at the fin edge zone and for higher slope film profiles in comparison of smaller slopes.

This effect is shown in Fig. 4.17 for $\Delta T = 0.6°C$ and for three different complementary angles. Predictions of (YL) and (A-YL) models are almost overlapping for entire range of the film thickness referring to Fig. 4.17 except for the small proximity before the fin edge. The blown up view shows that at the fin edge, for the case of $\theta = 20°$, the film thickness at the edge (δ_{edge}) is $\sim 0.05\mu$m

and the predictions of the (YL) and (A-YL) are close. This difference between two models becomes more obvious by increasing the magnitude of the complementary angle. In the case of $\theta = 40.301°$, since the film thickness reaches extremely smaller magnitudes, this mentioned difference between two models is at its maximum point. This further shows that the effect of disjoining pressure is non-negligible for small film thicknesses. Since the effect of disjoning pressure is more dominant at the fin edge and the film thickness at that point, (δ_{edge}), the variation of (δ_{edge}) with the complementary angle for various interface-wall temperature differences is plotted in Fig. 4.18. Predictions of film profile shows that, while the film thickness ath the edge zone is thick and slope is flatter, (YL) and (A-YL) are similar. By increasing the complementary angle, rendering the film thickness to become thinner at the edge, effect of disjoniig pressure intensifies and a separation between two models results emerges. The model with the disjoining pressure,(A-YL), results can only be obtained until a specific value of the complementary angle for a given temperature difference, beyond which no solution can be found. This cited limitation does not exist for (YL) model, and any specific complementary angle film profile could be obtained by using this model. This limitation point which occurs for (A-YL) model, is named as the “cut-off point" in the current study.

The main difference between (A-YL) and (YL) models is due to the cut-off point which exists in the results of (A-YL) model. Fig. 4.18 shows that, (YL) model can predict results for all values of complementary angles, unlike (A-YL). The results of (A-YL) model on the other hand, are limited by complementary angle. This limitation emerges when the film is thin enough to render disjoining pressure to be dominant. The variation of this cut-off point for four temperature differences is shown in Fig. 4.19. Total pressure gradient consists of terms, related to capillary and disjoning pressure, and existence of the cut-off point is due to these cited terms. Contribution of capillary and disjoinig pressure on the total mass flow rate solely is plotted in Fig. 4.20. This figure shows the contribution of terms corresponding to the case plotted in Fig. 4.19 for a temperature difference of $\Delta T = 0.03°C$, where the cut-off point is at $\theta_c = 10.4791°$. At the point away from the cut-off point when complementary angle

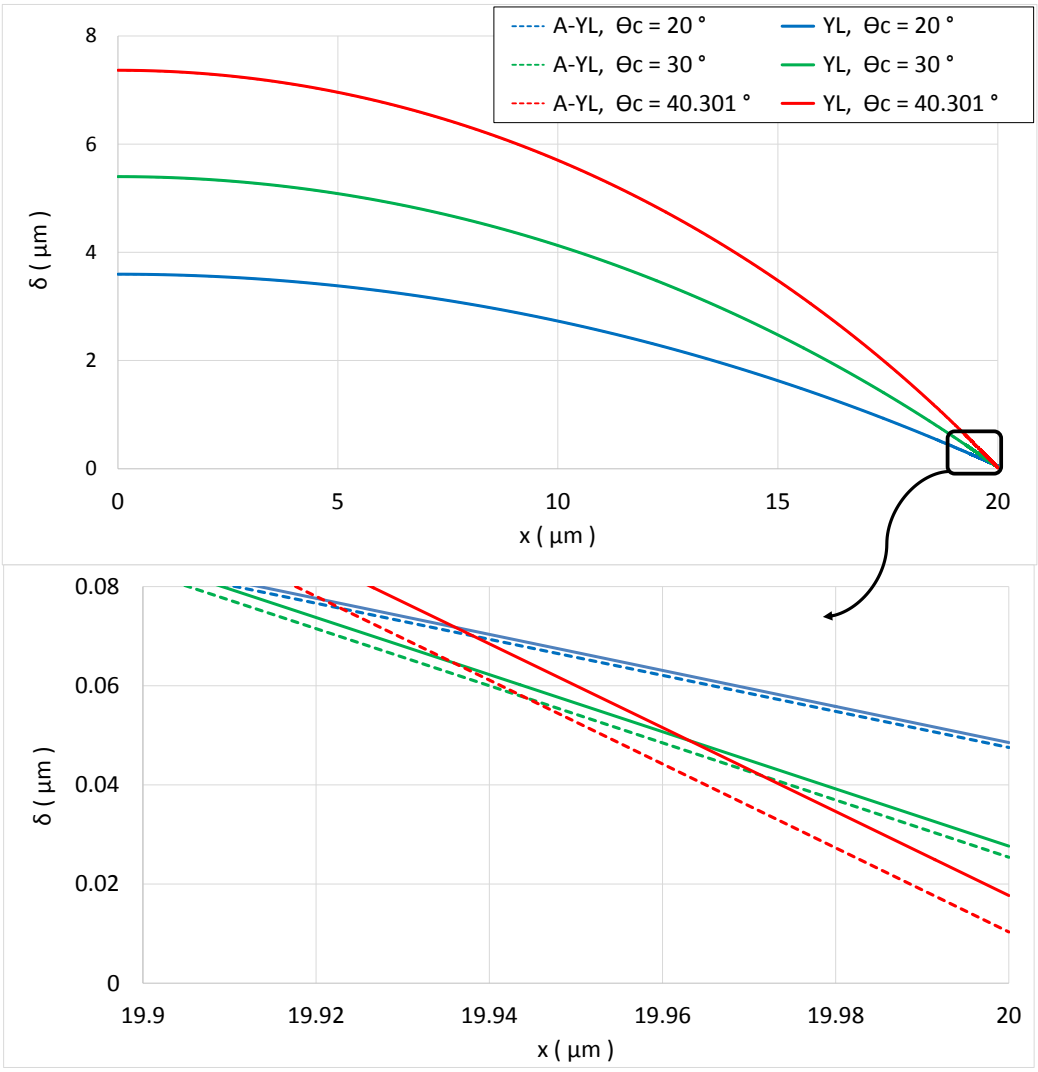

Figure 4.17: Film thickness in the vicinity of groove for (A-YL) and (YL) models at $\Delta T = 0.6°C$

is equal to $\theta_c = 8°$, dominant term contributing on the total pressure gradient and consequently on the mass flow rate is caused by capillary pressure. By increasing the magnitude of the complementary angle, and approaching to the cut-off point, the contribution rate of the disjoning pressure terms on the total mass flow rate increases due to the decrees in the film thickness at the fin edge. In case the results of $\theta_c = 8°$, $\theta_c = 10°$, $\theta_c = 10.4°$ and $\theta_c = 10.4791°C$ cases are compared, it can be understand that, when the point is away from the cut-off capillary pressure is dominant, in contrast, by approaching to cut-off point, disjoning pressures contribution increases and surpass the capillary pressure contribution. Finally, capillary pressures contribution fall into zero at the cut-off point, $\theta_c = 10.4791°$, and at this point the dominant terms refer to

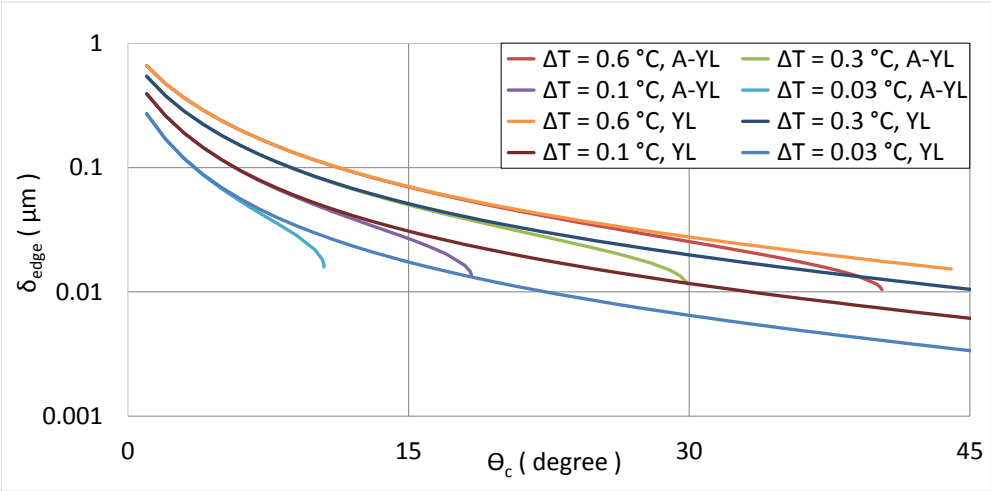

Figure 4.18: Variation of δ_{edge} with edge slope angle for (A-YL) and (YL) models

disjoning pressures contribution. By using Equations (3.10) and (3.12), mass flow rate expression for capillary pressure could be written as

$$m'_{P_c} = -\frac{1}{3\nu}\left(\frac{\sigma\delta_{xxx}}{\left(1+{\delta_x}^2\right)^{3/2}} - \frac{3\sigma\delta_x{\delta_{xx}}^2}{\left(1+{\delta_x}^2\right)^{5/2}}\right)\delta^3, \tag{4.2}$$

and for disjoining pressure the mass flow rate is equal to

$$m'_{P_d} = -\frac{1}{3\nu}\left(\frac{dP_d}{dx}\right)\delta^3. \tag{4.3}$$

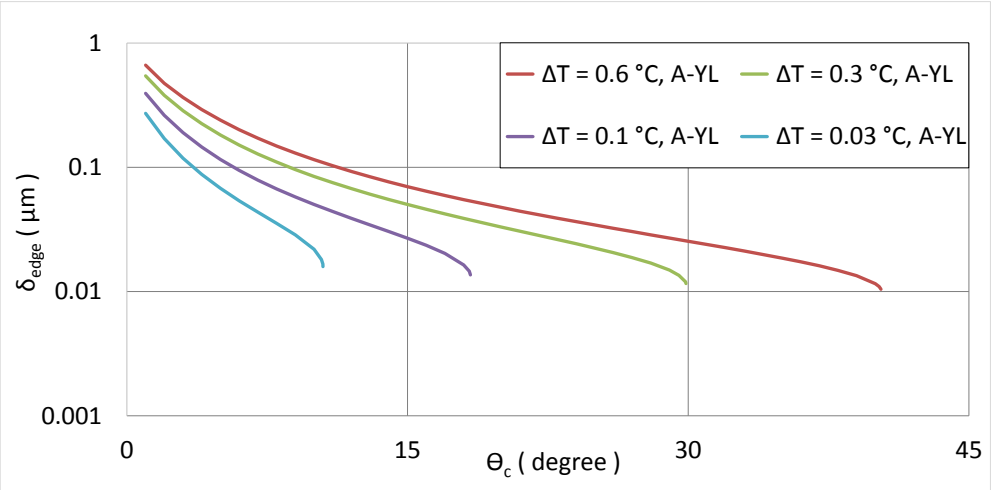

Figure 4.19: Variation of δ_{edge} with complementary angle for (A-YL) model

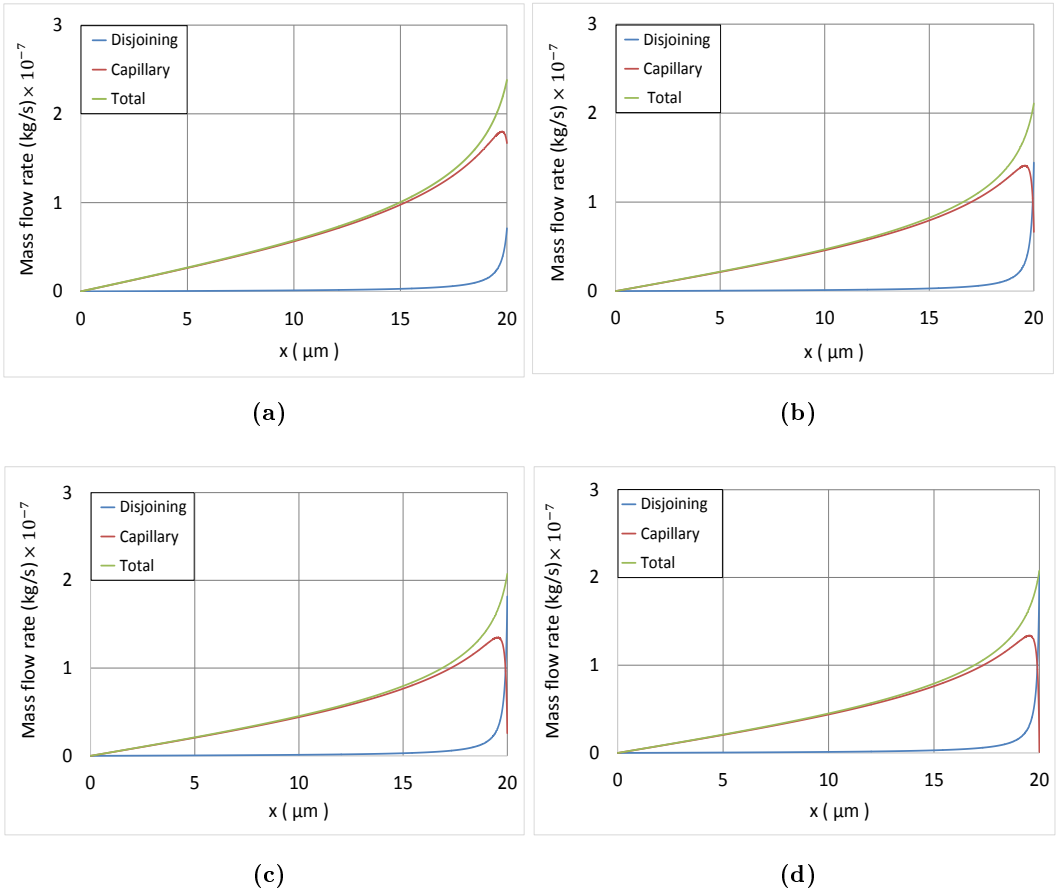

Figure 4.20: Contribution of capillary and disjoining pressure gradient terms to the mass flow rate for (a) $\theta_c = 8°$ (b) $\theta_c = 10°$ (c) $\theta_c = 10.4°$ (d) $\theta_c = 10.4791°$ at cut-off

The contribution of capillary pressure on the mass flow rate, m'_{cp}, is plotted with different temperature differences for (A-YL) and (AY) models. The magnitude of m'_{cp} in (YL) model, goes to zero smoothly with respect to the decline in the magnitude of temperature difference. Despite the (YL) model, in (A-YL) the magnitude of m'_{cp} drops radically near to the cut-off point.

The mass flow rate is proportional to the pressure gradient and the cross sectional area, effectively the film thickness. based on Fig. 4.20, by exceeding the cut-off point, it can be estimated that the magnitude of the capillary pressure becomes negative. Since in Eq. (4.2) the second term of the equation is always positive, this implies that negative contribution of capillary pressure requires $\delta_{xxx} = 0$ before the fin edge and $\delta_{xxx} < 0$ at the fin edge. Boundary conditions at the fin edge, forced the film profile's second derivative to be zero at the fin edge in order

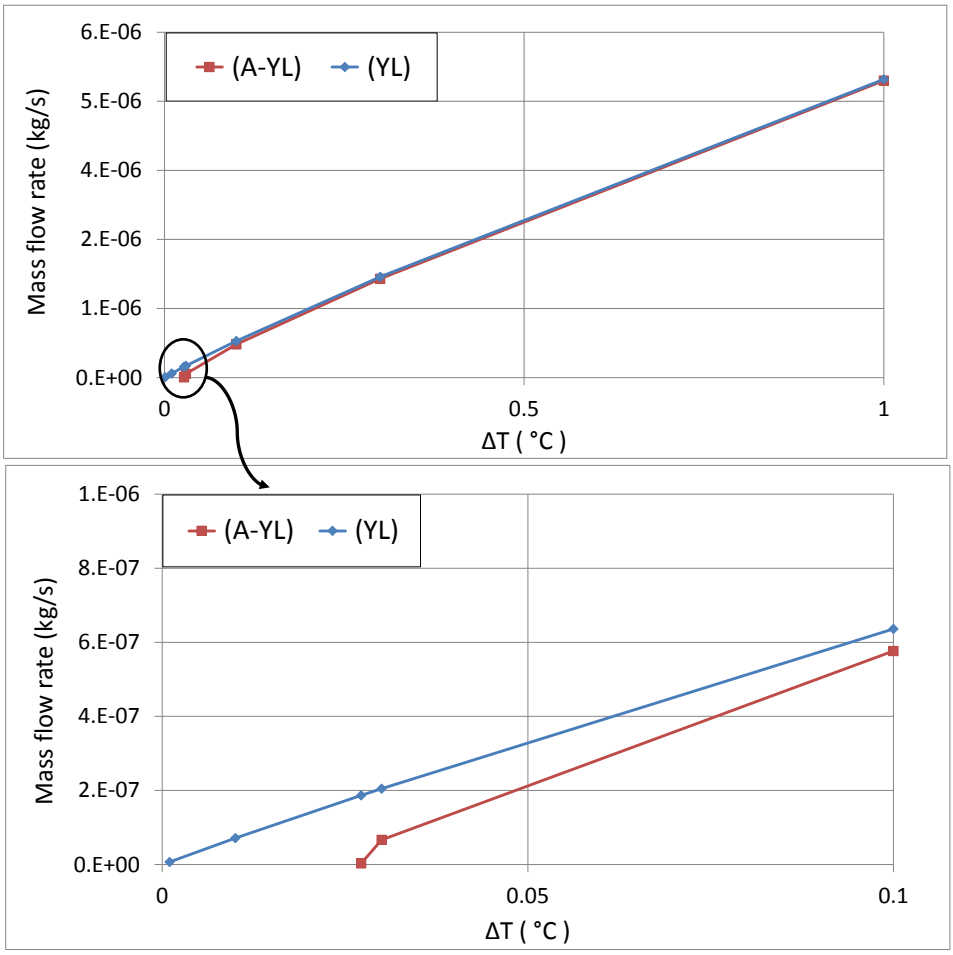

Figure 4.21: Mass flow rate percentage difference for (A-YL) and (YL) models

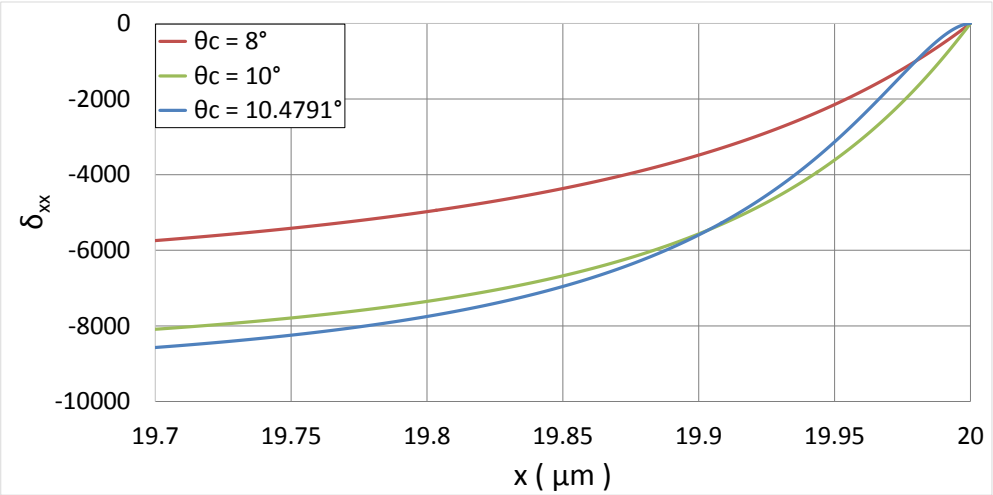

(a) Second derivative

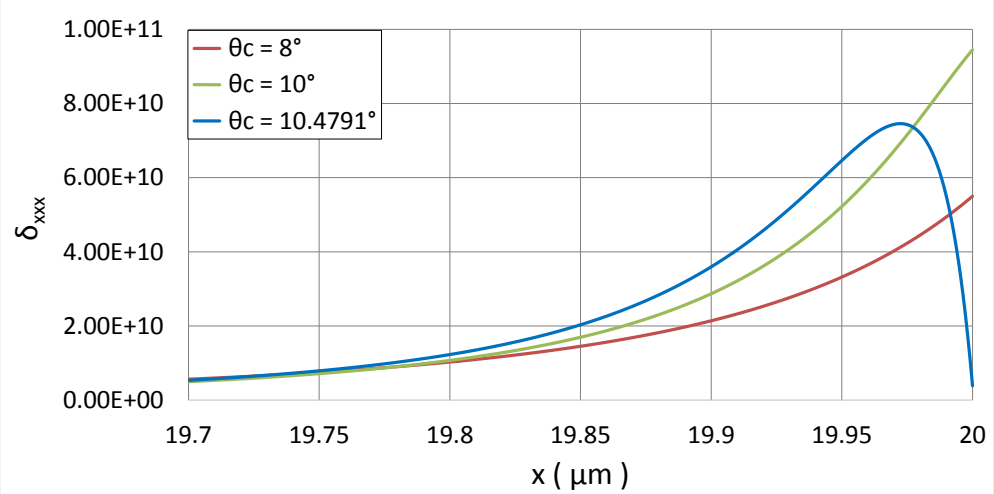

(b) Third derivative

Figure 4.22: Variation of δ_{xxx} and δ_{xx} of the δ_{edge} for $\Delta T = 0.03°C$

to match the groove profile. Since the second derivative of the film profile before the edge is negative, its gradient which is δ_{xxx} could not be negative if it should be vanished at the fin edge and reach zero from a negative value. Consequently a solution cannot be found for this case. This brings a limitation to the maximum value of the complementary angle for a given temperature difference. In the case of the (YL) model, where only the capillary term is present, no such limitation exists, since flow is due to the δ_{xxx}, which cannot approach zero, rendering solutions for all values of complementary angle θ_c. The behavior of the δ_{xxx} and δ_{xx} of the (δ_{edge}) is plotted in Fig. 4.22.

4.5 Effect of matching conditions and edge slope angle

Very few number of reports regarding the experimental results of the condensation film is available in the literature. In 2010, Lefèvre et al.[5] reported both experimental and numerical data for the condensation film on the fin top of a grooved heat pipe. Substantial difference between two set of results was reported in their paper. Their experimental test, which was conducted by using confocal microscopy, shows that the common set of boundary condition (Eq. (3.26)) may not always be valid due to the different matching condition that was observe din their test. This experimental result showed a inflection point of the fin profile located in a point before the fin edge and a slope break happened at the fin edge where the slope of the liquid film on the fin top did not match the slope of the liquid inside the groove. This point was reported in approximately 320 μm from the plane of symmetry. The authors argue that one of the reasons for this behavior may be attributable to the possible effect of van der Waals forces in the regions where the film is thin.

The current model is exercised in two different sets of boundary and interior conditions; one using the set of Eq. (3.26); and a second one using the set of Eq. (3.27)in which x_i refers to the interior inflection point before the fin edge, to simulate the experimental findings.

Thermophysical properties of the materials and geometry details that were used in [5] are applied and implemented in this study. Groove width and radius of curvature are 400 μm and 1.08 mm, respectively. This radius makes the complementary angle to be equal as 10.68°. By applying the same properties of [5] and using the first set of boundary conditions (Eq. (3.26), results are obtained and a comparison between the experimental data and the numerical predictions is plotted in Fig.4.23 (a). There is a substantial different between the results, and the shape of the profiles do not match each other. As a result, in order to match the profiles, lower heat fluxes were exercised but matching did not happen in those cases either. The reason of this noticeable difference between film shapes of experimental and theoretical result refers to the boundary conditions defined in Eq. (3.26). Because of the imposed first and second derivative located exactly at

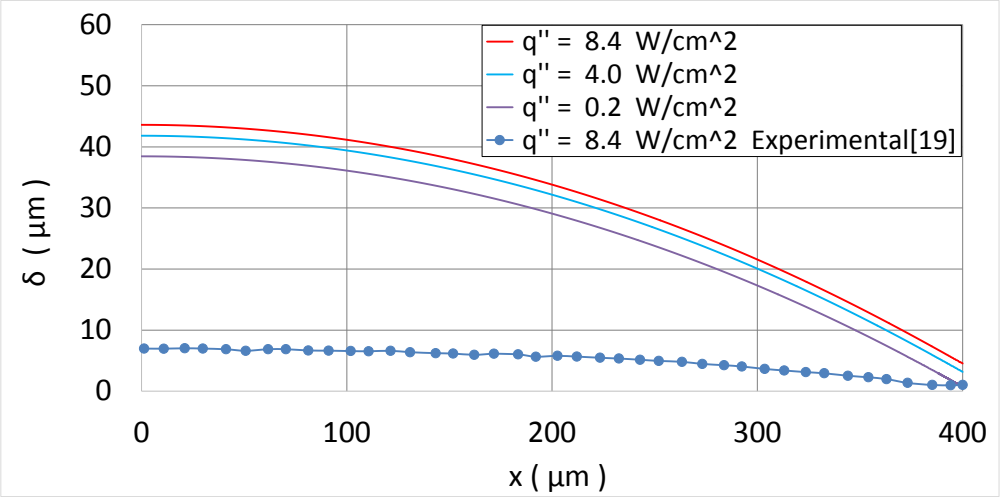

(a)

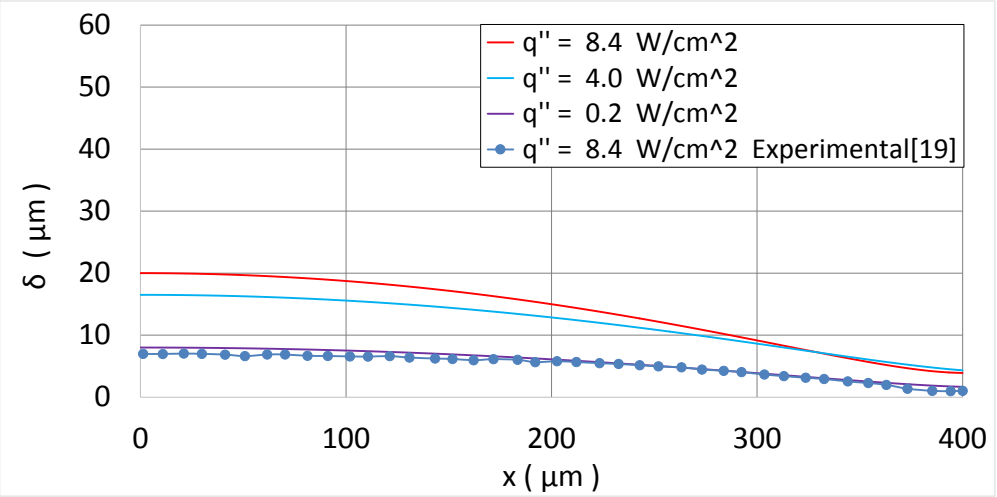

(b)

Figure 4.23: (a) Comparison of results using Eq. (3.26) and experimental data of [5] (b) Comparison of results using Eq. (3.27) and experimental data obtained in [5], where the inflection point in the profile is at $x_i = 320\ \mu$m

the fin edge, the shape of the film profile remains unchanged for different range of inputted heat fluxes. The same manner is observable for constant temperature difference boundary condition as plotted in Fig. 4.4.

Comparison between experimental and theoretical results shows that by using boundary conditions defined in Eq. (3.26), matching between these results is unattainable. In this study, disjoning pressure—effectively van der Waals term—is included in the modeling process, but this inclusion does not help the numerical results to match the experimental observations either. Second set of boundary consitions defined in Eq. (3.27) applied to the model, in order to compare the new results with experimental observation of [5]. This comparison is given in Fig. 4.23 (b). Unlike Fig.4.23 (a) a reduction in the magnitude of the heat flux changes the magnitudes of the film thickness ultimately matching the experimental, albeit at a much lower heat flux of 0.2 W/m^2. Possibility of the parallel flow on the fin top and in the direction of groove, was suggested by Lefèvre et al.[5] as a second reason for the discrepancy between their experimentally measure and simulation results. The fact that the matching of experimental measurements and current study exists at lower heat fluxes may also be due to the possible presence of such a flow. In summary, the second set of boundary conditions at the fin edge enabled the matching of the general character of the liquid film, and the magnitude of the heat transferred through the film resulted in the matching of the entire profile. This cited parallel flows have been neglected in the previous studies of condensation films up to date.

4.6 Double solution with (A-YL) model

The results of general differential equation Eq. (3.25) shows a double solution manner (bifurcation) which means there are two different and independent results for exactly same set of physical inputs and boundary conditions. The effects of disjoning pressure is more significant where the thickness of the film is thinner, which occurs at the ending zone of the film and near to the edge of the fin. The results for (δ_{edge}), which is the magnitude of the film thickness at the fin edge, are shown in Fig. 4.24 with different θ_c and ΔT. Bifurcation

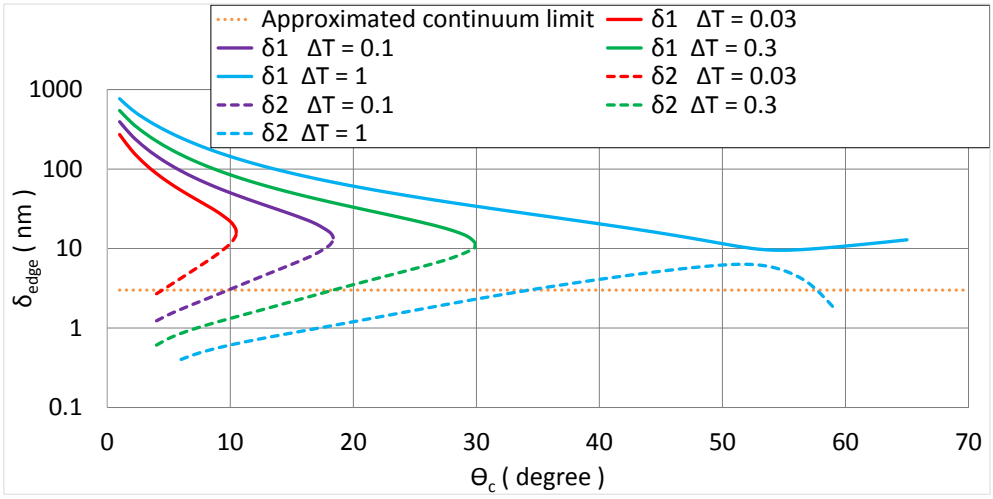

Figure 4.24: First and second set of results for (δ_{edge}) with different θ_c and ΔT while the full form of P_d is used

manner of results are shown in Fig. 4.24, where results with higher magnitude for (δ_{edge}) are named as "first answer" and shown as (δ_1). Another set of results are named as "second answer" and shown as (δ_2). These bifurcation manner happen regardless of which type of disjoining pressure, presented in modeling section, is being used.

Since δ_2 results in a highly small magnitudes for (δ_{edge}), approximated limit for continuum postulate is added to the Fig. 4.24 in order to check the physical validity of the results. Although all the data are mathematically valid and true, but their physical availability should be carefully taken into consideration. The first step for examining the physical availability is checking the continuum limit for the data. it could be concluded that the (δ_{edge}) located under the approximated continuum line could not be acceptable. The second factor for examining the physical availability is the existence of negative absolute pressure. Extremely small film thicknesses will cause the disjoning pressure to reach noticeable higher magnitudes which could cause the absolute pressure to be negative, which is not physically sensible. The limit of this factor is almost the same as the continuum limit, which again means that the (δ_{edge}) located under that approximated limit could not be acceptable. For physical validation of the data located above this limitation line and resulted by second set of data, other examining factors like the matching condition between the film and liquid inside the groove and

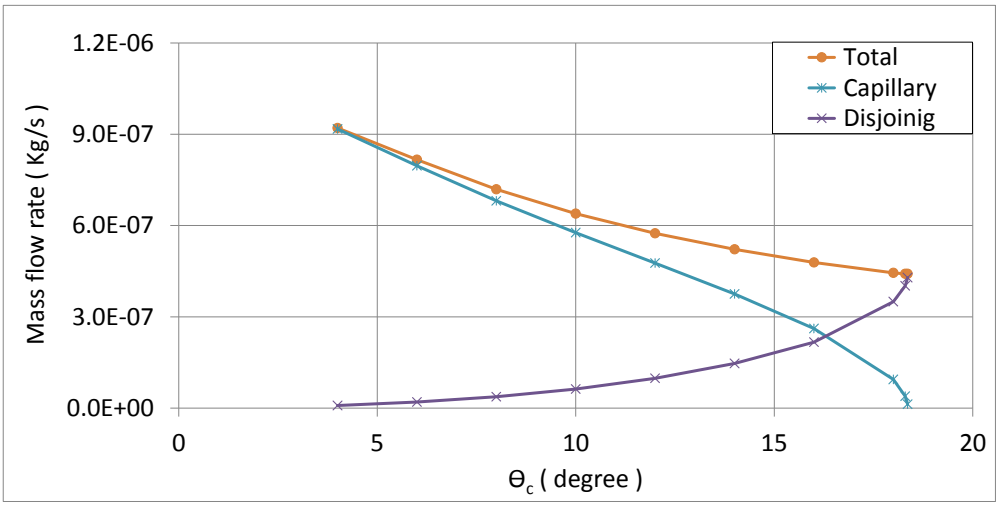

(a) First answer

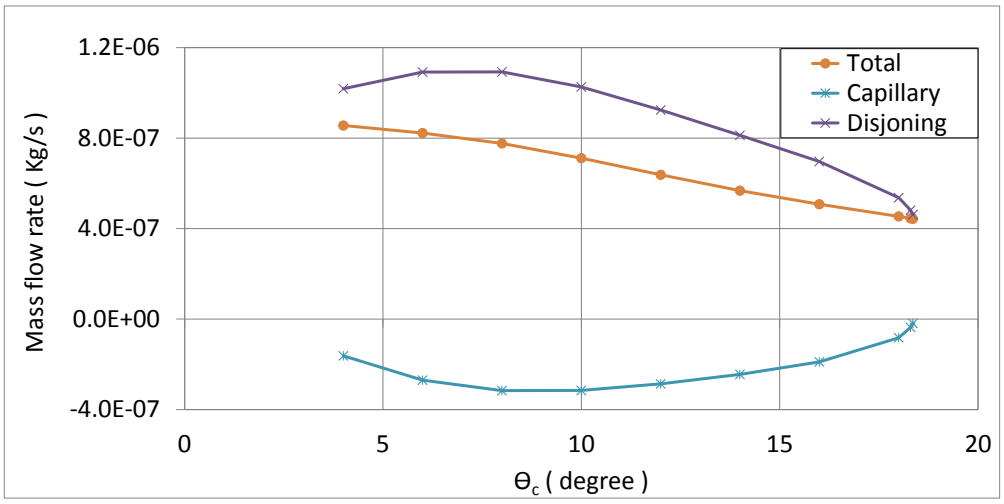

(b) Second answer

Figure 4.25: Mass flow rate contribution of capillary and disjoining pressure on the total mass flow rate for $\Delta T = 0.03°C$

continuity of the film profile at that spot should be analyzed. This discussion is further presented at the end of this section.

The results shows a limitation point where both set of answers are converged into the one point, these limitation points emerge because of the presence of dosjoinig pressure and are named as cut-off points. While the disjoning pressure is excluded from the augmented Young-Laplace equation, this cited cut-off points are vanished and model will have results without any restriction by θ_c. The contributing factors which make the profile to results in these cut-off points are discussed in section 4.4 . In order to have a better insight into the reasons behind this bifurcation manner, the contribution of the capillary and disjoning pressure on the total mas flow rate for both answers with different θ_c are plotted in Fig. 4.25. Adding disjoining pressure terms to the Young-Laplace equation, brings an opportunity for disjoining pressure to have a balancing contribution with capillary pressure on the total generated mass flow rate. In Fig. 4.25 (a) which is related to first set of answers, the capillary pressures contribution magnitude is almost the same as the total amount in the flatter zones. But by approaching to the cut-off point the disjoining pressure become more dominant, rendering the capillary pressures contribution to fall into zero. In contrast of the disjioning pressures contribution pattern in the first set of answers, its magnitude starts with a higher value than the total mass flow rate, implies the point that capillary pressure should start from negative spot. This pattern is shown in Fig. (b), where by approaching to the cut-off point the magnitude of the contribution of capillary pressure goes to zero and the total and disjonig pressure converges.

This thinner thickness that is essential for providing the required magnitude for disjoning pressure in second set of answers makes the film profiles of the same θ_c to be significantly different, especially for the cases where complementary angle is not near to the cut-off point. Contribution of the capillary and disjoning pressure on the total mass flow rate along the fin top is plotted in Fig. 4.28 for four different θ_c. These selected complementary angles are shown in Fig. 4.27 as red spots, The same θ_c was chosen for plotting the same figure for first set of answers in Fig. 4.20. Those shown in orange color are referring to the complementary angles used in plotting Fig. 4.20.

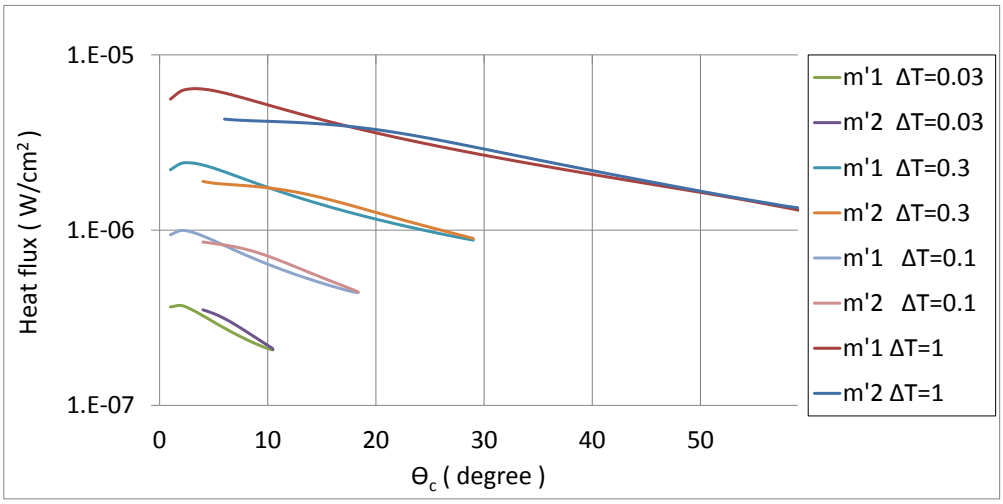

Figure 4.26: Heat flux difference between the results of first and second set of answers

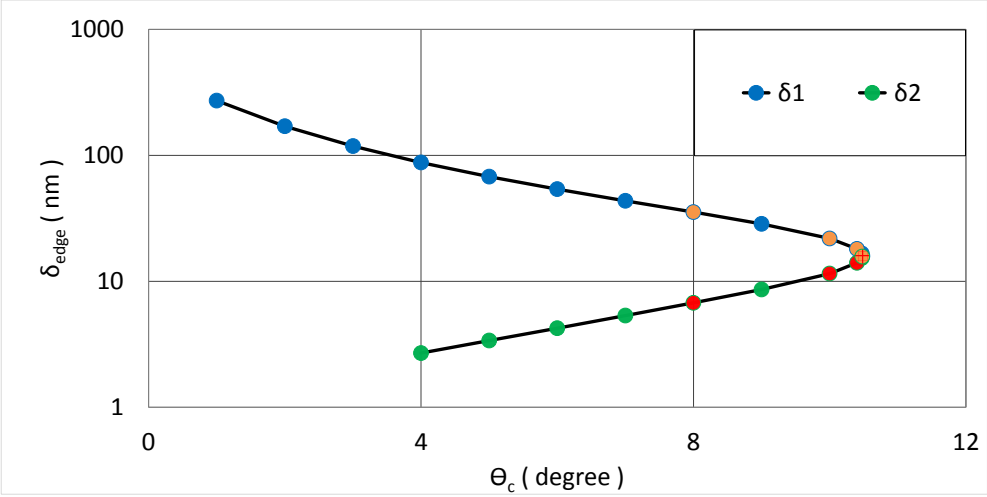

Figure 4.27: First and second set of results for δ_{edge} for $\Delta T = 0.03°C$, showing the points selected for analyzing the pressure gradient contribution to mass flow rate presented in Figs. 4.28 and 4.20, red ones are used in Figs. 4.28 and orange ones are used in 4.20

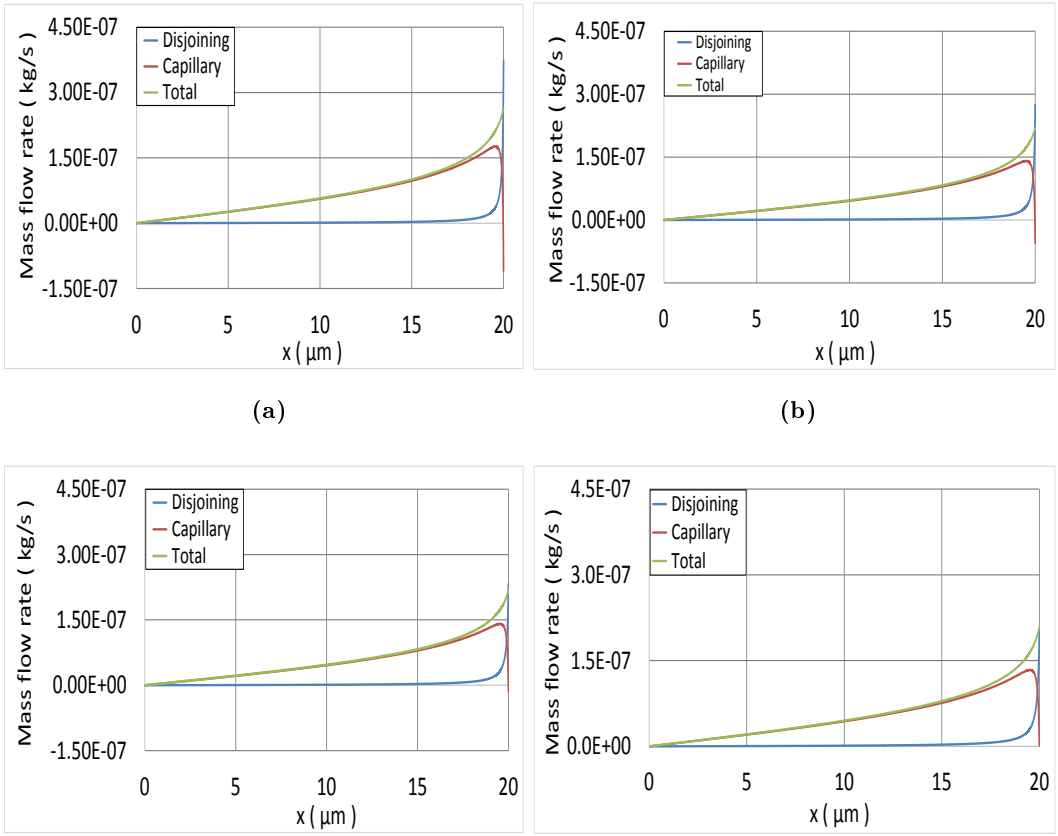

Figure 4.28: Contribution of capillary and disjoining pressure gradient terms to the mass flow rate for (a) $\theta_c = 8°$ (b) $\theta_c = 10°$ (c) $\theta_c = 10.4°$ (d) $\theta_c = 10.4791°$ at cut-off in second set of answers

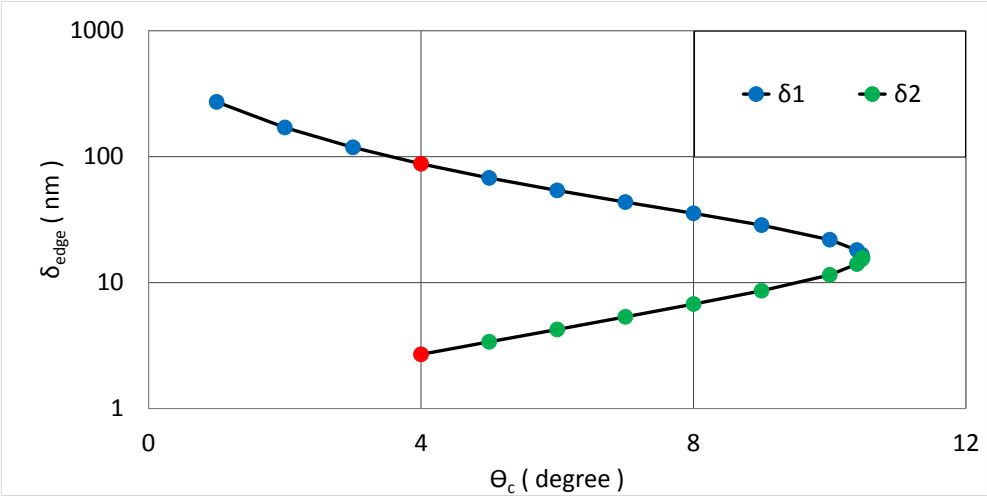

(a)

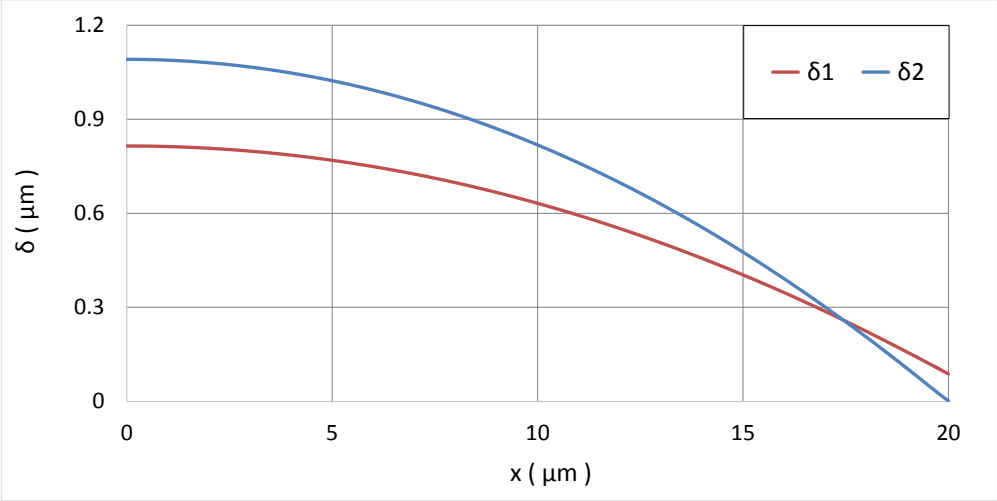

(b)

Figure 4.29: (a) δ_{edge} results when $\Delta T = 0.03°C$ (b) Comparison of film thickness for first and second set of results for $\Delta T = 0.03°C$ and $\theta_c = 4°$

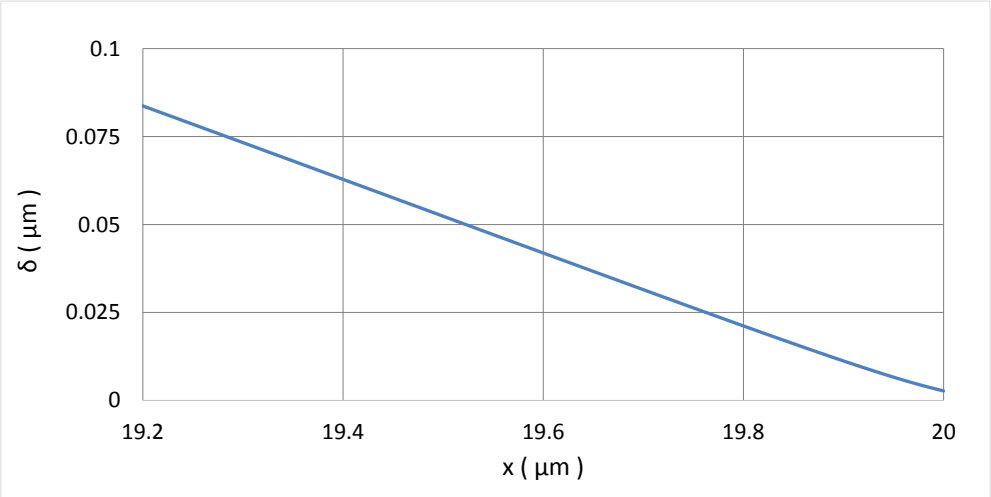

Figure 4.30: Second set of results film thickness profile when $\Delta T = 0.03°\text{C}$ and $\theta = 4°$

Fig. 4.28 shows that by approaching to the cut-off point m'_{P_c} reaches zero from a negative spot rendering the m'_{P_d} to match the total mass flow rate. Although the profiles are demonstrating different shapes, because the imposed temperature differences between wall and the vapor is equal for both answers, resulting mass flow rates are almost the same. This point is expressed in Fig. 4.26. Shape of the film profiles for two set of answers are plotted in Fig. 4.29 for $\theta_c = 4°$ and $\Delta T = 0.03°\text{C}$. The negative sign of the mass flow rate contribution of capillary pressures in the second set of answers, suggests that the sign of the film's arc should be positive which demands a positive δ_{xx}. Since the third derivative is negative, $\delta_{xxx} < 0$, in this set of answers, the change in sing of second derivative is necessary in order to satisfy the boundary condition at the fin edge ($\delta_{xx} = 0$). By magnifying the ending zone of the film profile of second set of answers in Fig. 4.29, where the disjoining pressure is dominant in both set of answers, this change in the second derivatives sign could be observed and is plotted as Fig. 4.30. It can be deduce that by exceeding the cut-off point, the capillary pressures contribution will be positive which means $\delta_{xxx} > 0$. Since both δ_{xx} and δ_{xxx} will be positive in that case, the $\delta_{xx} = 0$ at the fin edge could not be satisfied and consequently, solution can not be found. The variation of δ_{xx} and δ_{xxx} is plotted in Fig. 4.33.

Previously, two factor for validating the physical availability of the results, more especially the second set of results, were introduced. The another parameter that

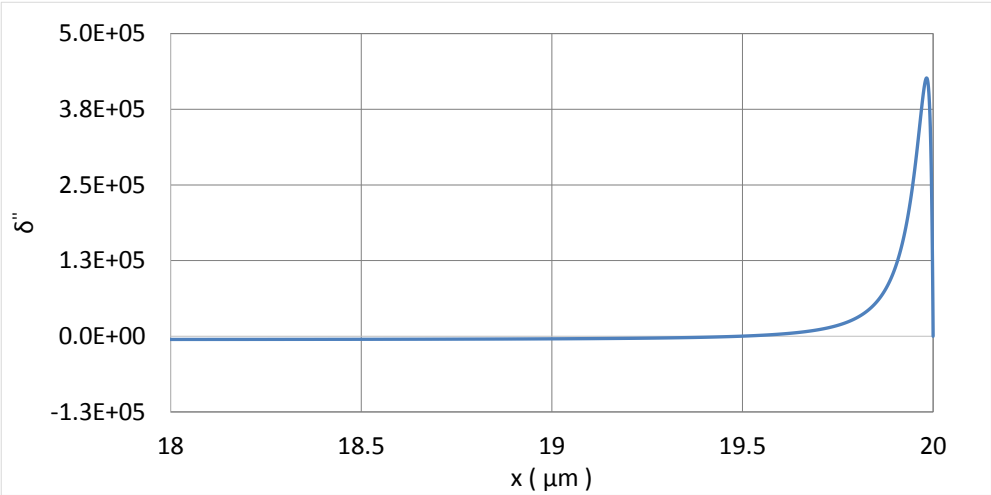

(a)

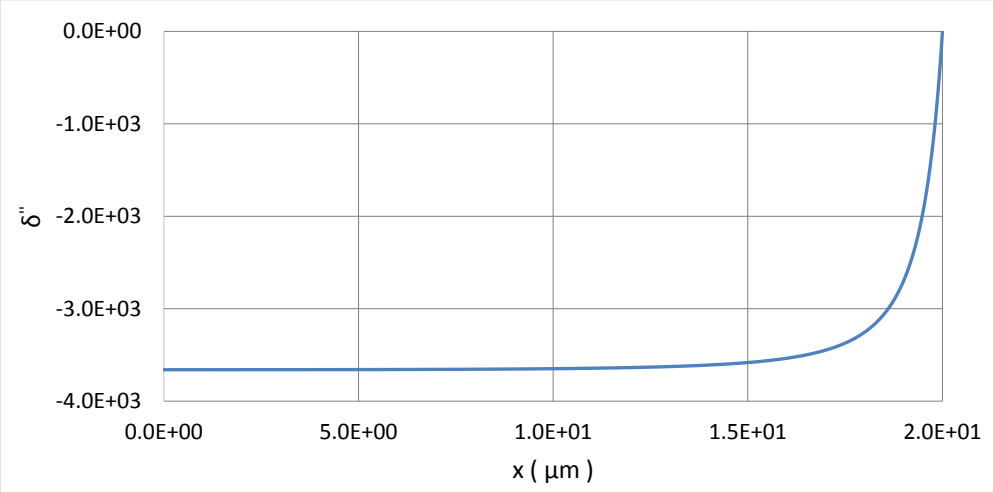

(b)

Figure 4.31: (a) δ_{xx} when $\Delta T = 0.03°\text{C}$ and $\theta = 4°$ for second set of answers (b) δ_{xx} when $\Delta T = 0.03°\text{C}$ and $\theta = 4°$ for first set of answers, red points in Fig. 4.29

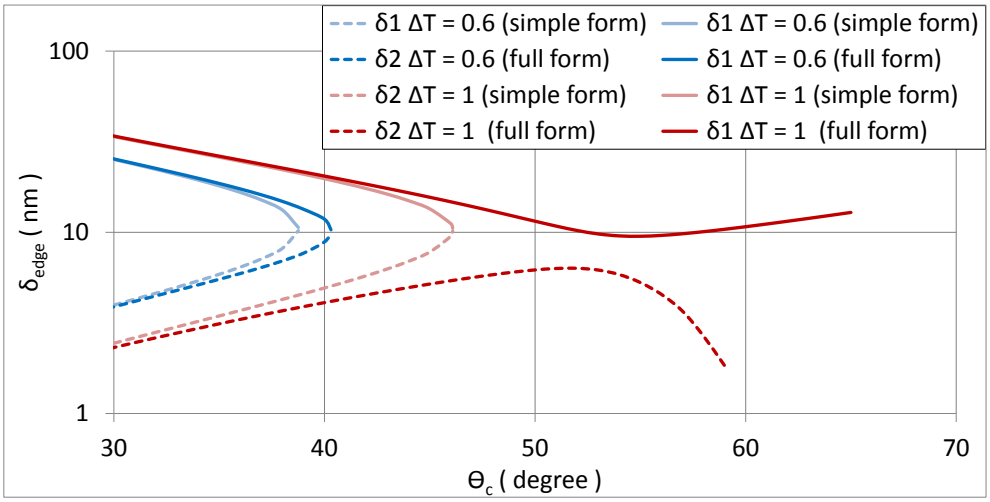

Figure 4.32: Comparison between First and second set of results for different complementary angles for full and simple form of disjoning pressure

should be taken into consideration is the continuity of the film at the matching point with the liquid inside the groove. Fig. 4.31 presents the δ_{xx} profiles of the both answers. The first answers second derivative is always negative and finally reaches zero at the fin edge zone as the boundary condition imposes. The second set of answers, as it is mentioned previously, must have positive second derivative at the ending zone of the fin. This positive derivative radically reaches zero because of the boundary condition at the edge. This studies modeling is only predicting the film profiles before the fin edge, but as it can be estimated, the liquid inside the groove has a positive arc which needs a positive second derivative. If the film profile have a positive second derivative after the fin edge, the second answer could not be valid because it can cause non-continuity at that zone, since just before the edge it radically reaches zero. In contrast of this manner, the first set of answers never show any non-continuity because its second derivative reaches zero from a negative spot and can continue to positive spot smoothly.

Despite the convergence manner of the results and the existence of cut-off points, the code results in a divergence manner in a higher temperature differences. This manner does not happen while the simple form of disjoinig pressure is being used. This difference is shown in Fig. 4.32. The main reason behind this divergence manner is based on the higher order derivatives which the full form contains,

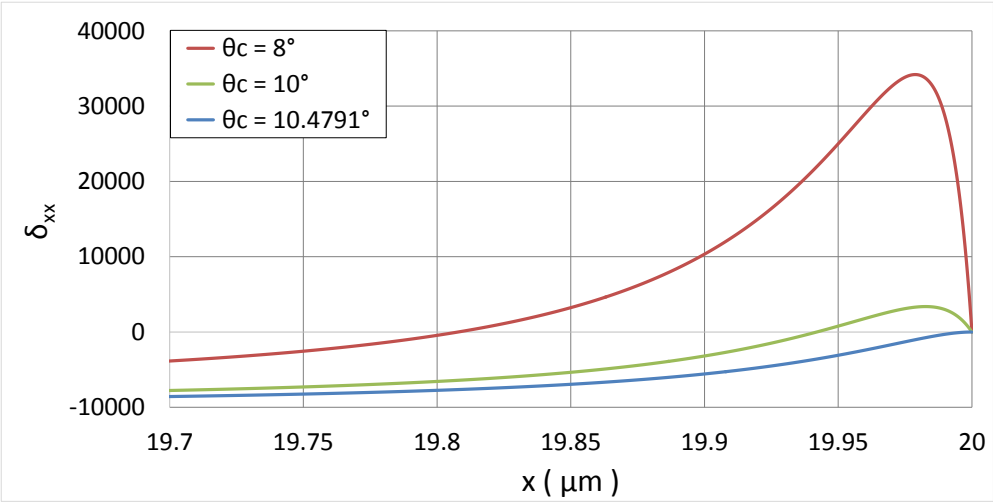

(a) Second derivative

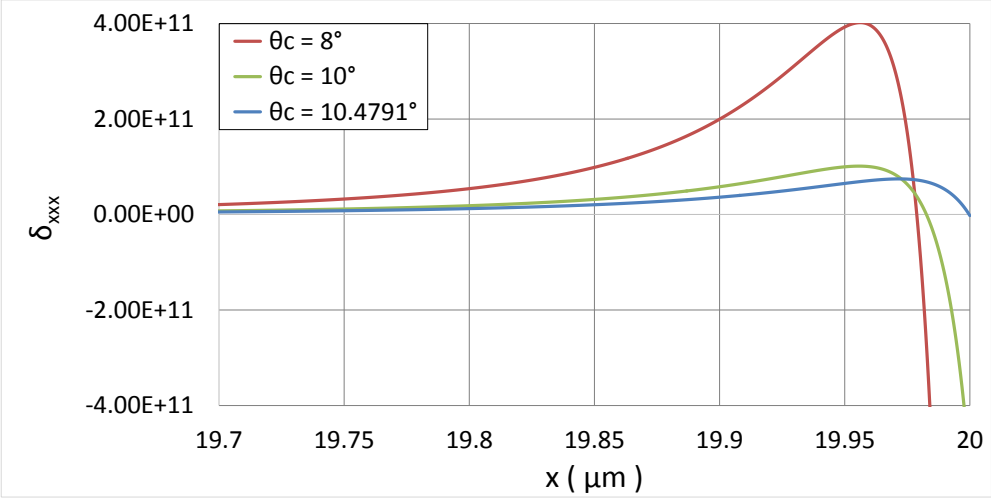

(b) Third derivative

Figure 4.33: Variation of δ_{xxx} and δ_{xx} of the δ_{edge} for $\Delta T = 0.03°C$ for second set of answers

despite the the simple form which does not include any derivative terms.

The dispersion constant A, used in the "Full model" form of the disjoning pressure at Eq. (3.22) was obtained from [20], but the value of B was calculated based on the van der Waals potentials and molecular densities for water. In order to better understand the effect of these two constant on the behavior of the model, different values of them with referencing the initial magnitudes named as A0 and B0 are plotted in Fig. 4.34 . Although the values of the (δ_{edge}) for different A and B could be different, the basic manner of the condensation film, cut-off and bifurcation, are same in all cases. By analyzing the Fig. 4.34 it could be understood that the magnitude of the cut-off point is increasing by the using a higher value for B. In contrast, this cut-off point is decreasing by increasing the magnitude of the A.

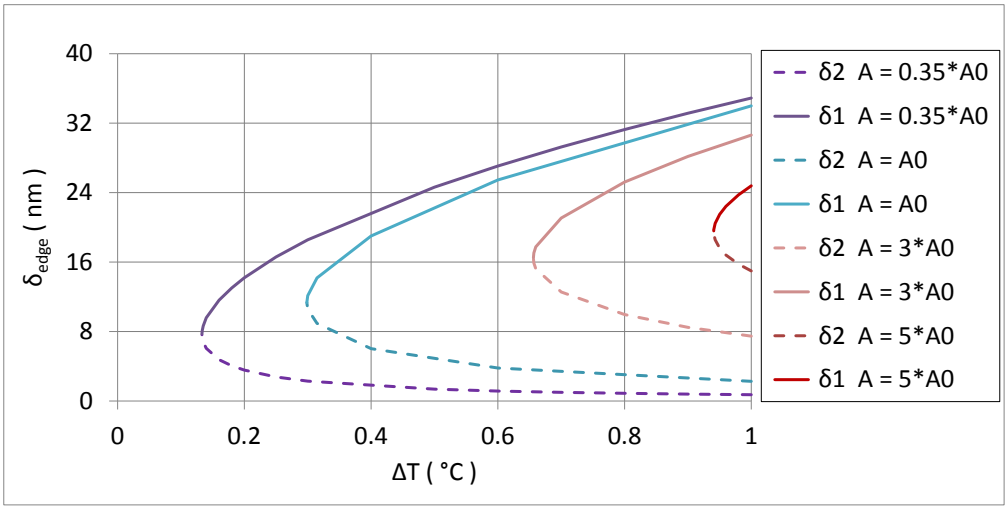

(a)

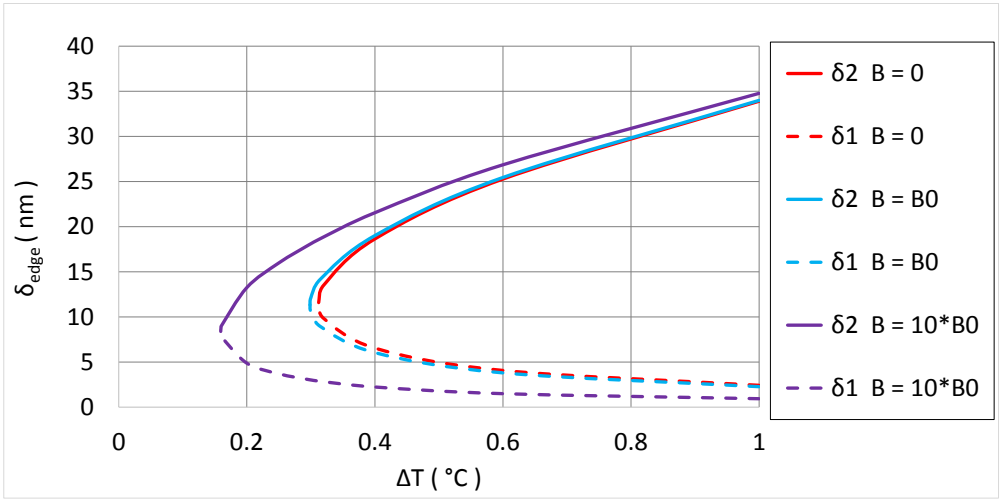

(b)

Figure 4.34: (a) Comparison between δ_{edge} results for different A values (b) Comparison between δ_{edge} results for different B values

CHAPTER 5

SUMMARY AND FUTURE WORK

5.1 Conclusion

Governing equation of the condensation film on the fin top of the grooved heat pipe including the effects of disjoinig pressure is solved numerically and the different comparisons and discussions took place in this study. Neglecting the disjoning pressure could result in over predicting the film thickness for wider range of complementary angles, since the cut-off points appear while the disjoinig pressure is included. Validation between experimental and theoretical results, suggested that the set of boundary conditions commonly used in literature could not be always valid. The alternative set of boundary conditions were assumed which resulted in better compatibility with the experimental data. Bifurcation is happening while the disjoning pressure is included to the condensation modeling, but the second set of answers which result in more thinner magnitudes for δ_{edge} was not physically approved after examinations. The main conclusions and bold findings of this study could be summarized as below:

- Specification of edge angle dictates the shape and thickness of film
- Effect of disjoining pressure is important for small film thickness
- Effect of disjoining is restricted to fin edge for large edge angles, due to sudden increase of thickness away from the edge
- With disjoining a cut-off exist in solutions when assumptions in the literature for matching with the groove are used
- Assumptions used in matching with the groove may not always be valid

- With disjoining a bifurcation manner exists for the results
- Although bifurcations two different set of answers are mathematically valid, but examinations prove that the physical availability of the second set of answers is not predictable

Possibility of parallel flow, which its existence was discussed in the section 4.5, should be taken into account in future modelings. Future works for improving the condensation model is discussed in further sections.

5.2 Possible future work

5.2.1 Effect of surface roughness

Surface roughness could play a great role on the behavior of the film regarding its thin thickness especially at the fin edge zone. In this study the surface was considered as ideal, but the surface roughness could readily render a notable change in the effect of the disjoining pressure and consequently on the behavior and shape of the liquid film on the fin top.

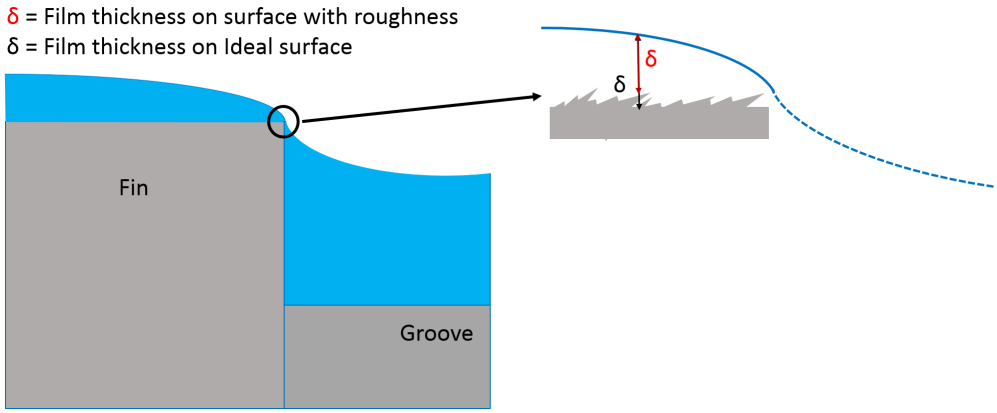

Figure 5.1: Surface roughness effect on the liquid film

In the fin edge zone, where the film thickness is thinner the effect of surface roughness is more important. Film thickness at the edge which is utterly dependent on the contact angle but normally is in the range of 1 - 100 nm and in this range surface roughness will have a great impact on the pressure balance,

slope and curvature of the film. Surface roughness range could be altered based on the manufacturing method that is used for creating grooves and fins in the heat pipe. Beside the manufacturing process, the materials which are chosen for the substances is another important factor for defining the range of surface roughness. The fact which is undeniable is its effect on the film profile since its magnitude will at least in nano scale. Fig. 5.1 shows a blown up schematic of the fin edge with surface roughness.

5.2.2 Recommendation for future work

The discussion presented in 4.5 referring to the validation between experimental and theoretical results, suggested that there is possibility for flow existence parallel to the groove. This concept should be added to the future modelings in order to better anticipate the sharing rate of the mass flow on the fin top in the direction perpendicular and parallel to the groove. This mentioned flow is shown in Fig. 5.2.

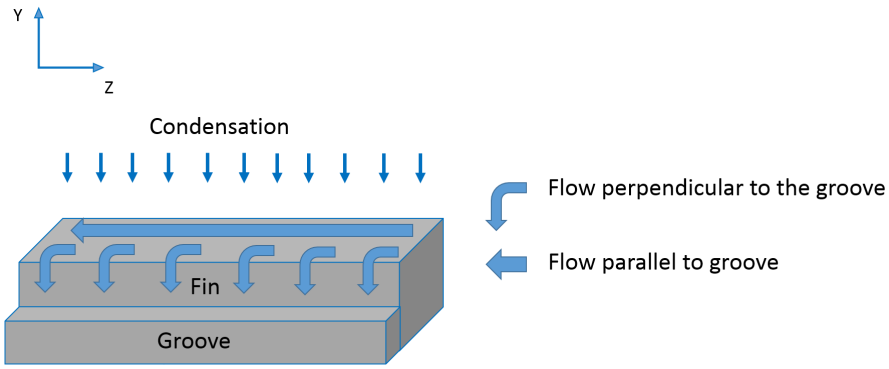

Figure 5.2: Possible low directions on the fin top

REFERENCES

[1] Heat Pipes and Vapor Chambers – What's the Difference? | Celsia, last visit: 03.10.2017. URL `http://celsiainc.com/blog-heat-pipes-and-vapor-chambers-whats-the-difference/`.

[2] A. Faghri. Heat Pipes: Review, Opportunities and Challenges. *Frontiers in Heat Pipes*, 5(1), 2014. ISSN 2155-658X. doi: 10.5098/fhp.5.1.

[3] Y. Akkuş. *Multi-dimensional modeling of evaporation in the micro region of a micro grooved heat pipe*. PhD Thesis, Middle East Technical University, 2015.

[4] A. Faghri, Y. Zhang. Numerical Simulation of Condensation on a Capillary Grooved Structure. *Numerical Heat Transfer, Part A: Applications*, 39(3): 227–243, 2001. ISSN 1040-7782. doi: 10.1080/104077801300006562.

[5] Fr. Lefèvre, S. Lips, and J. Bonjour. Investigation of Evaporation and Condensation Processes Specific To Grooved Flat Heat Pipes. *Frontiers in Heat Pipes*, 1(2), 2010. ISSN 2155-658X. doi: 10.5098/fhp.v1.2.3001.

[6] R Hopkins, A Faghri, and D Khrustalev. Flat Miniature Heat Pipes With Micro Capillary Grooves. *Journal of Heat Transfer*, 121(1):102–109, feb 1999. ISSN 0022-1481.

[7] M. Potash and P. C. Wayner. Evaporation from a two-dimensional extended meniscus. *International Journal of Heat and Mass Transfer*, 15(10):1851–1863, 1972. ISSN 00179310. doi: 10.1016/0017-9310(72)90058-0.

[8] P. C. Wayner and C. L. Coccio. Heat and mass transfer in the vicinity of the triple interline of a meniscus. *AIChE Journal*, 17(3):569–574, 1971. ISSN 15475905. doi: 10.1002/aic.690170317.

[9] P. C. Wayner, Y. K. Kao, and L. V. LaCroix. The interline heat-transfer coefficient of an evaporating wetting film. *International Journal of Heat and Mass Transfer*, 19(5):487–492, 1976. ISSN 00179310. doi: 10.1016/0017-9310(76)90161-7.

[10] R. W. Schrage. A theoretical study of interphase mass transfer., 1953.

[11] Z.M. Zorin, B.V. Derjaguin. Optical study of the adsorption and surface condensation of vapours in the vicinity of saturation on a smooth surface. In *Proc. 2nd Int. Congr. Surface Activity, London 2*, pages 145–152, 1957.

[12] A. Mirzamoghaclam and I. Catton. A Physical Model of the Evaporating Meniscus. *Journal of Heat Transfer*, 110(February):201–207, 1988. ISSN 00221481. doi: 10.1115/1.3250452.

[13] S. DasGupta, I. Y. Kim, and P. C. Wayner. Use of the Kelvin-Clapeyron Equation to Model an Evaporating Curved Microfilm. *Journal of Heat Transfer*, 116(November):1007–1015, 1994. ISSN 00221481. doi: 10.1115/1.2911436.

[14] P.C. Stephan and C.A. Busse. Analysis of the heat transfer coefficient of grooved heat pipe evaporator walls. *International Journal of Heat and Mass Transfer*, 35(2):383–391, 1992. ISSN 00179310. doi: 10.1016/0017-9310(92)90276-X.

[15] S. K. Wee, K. D. Kihm, and K. P. Hallinan. Effects of the liquid polarity and the wall slip on the heat and mass transport characteristics of the micro-scale evaporating transition film. *International Journal of Heat and Mass Transfer*, 48(2):265–278, 2005. ISSN 00179310. doi: 10.1016/j.ijheatmasstransfer.2004.08.021.

[16] H. Wang, S. V. Garimella, and J. Y. Murthy. Characteristics of an evaporating thin film in a microchannel. *International Journal of Heat and Mass Transfer*, 50(19-20):3933–3942, 2007. ISSN 00179310. doi: 10.1016/j.ijheatmasstransfer.2007.01.052.

[17] R. Bertossi, Z. Lataoui, V. Ayel, C. Romestant, and Y. Bertin. Modeling of Thin Liquid Film in Grooved Heat Pipes. *Numerical Heat Transfer, Part*

A: Applications, 55(March 2013):1075–1095, 2009. ISSN 1040-7782. doi: 10.1080/10407780903014228.

[18] S. Y. Du and Y. H. Zhao. New boundary conditions for the evaporating thin-film model in a rectangular micro channel. *International Journal of Heat and Mass Transfer*, 54(15-16):3694–3701, 2011. ISSN 00179310. doi: 10.1016/j.ijheatmasstransfer.2011.02.059.

[19] Z. H. Kou, H. T. Lv, W. Zeng, M. L. Bai, and Ji Z. Lv. Comparison of different analytical models for heat and mass transfer characteristics of an evaporating meniscus in a micro-channel. *International Communications in Heat and Mass Transfer*, 63:49–53, 2015. ISSN 07351933. doi: 10.1016/j.icheatmasstransfer.2015.02.005.

[20] K. H. Do, S. J. Kim, and S. V. Garimella. A mathematical model for analyzing the thermal characteristics of a flat micro heat pipe with a grooved wick. *International Journal of Heat and Mass Transfer*, 51(19-20):4637–4650, 2008. ISSN 00179310. doi: 10.1016/j.ijheatmasstransfer.2008.02.039.

[21] Y. Akkuş and Z. Dursunkaya. A new approach to thin film evaporation modeling. *International Journal of Heat and Mass Transfer*, 101:742–748, 2016. ISSN 00179310. doi: 10.1016/j.ijheatmasstransfer.2016.05.091.

[22] A. J. Jiao, R. Riegler, H. B. Ma, and G. P. Peterson. Thin film evaporation effect on heat transport capability in a grooved heat pipe. *Microfluidics and Nanofluidics*, 1(3):227–233, 2005. ISSN 16134982. doi: 10.1007/s10404-004-0015-6.

[23] F. Lefèvre, R. Rullière, G. Pandraud, and M. Lallemand. Prediction of the temperature field in flat plate heat pipes with micro-grooves - Experimental validation. *International Journal of Heat and Mass Transfer*, 51(15-16):4083–4094, 2008. ISSN 00179310. doi: 10.1016/j.ijheatmasstransfer.2007.12.007.

[24] K. Hyung Do and S. P. Jang. Effect of nanofluids on the thermal performance of a flat micro heat pipe with a rectangular grooved wick. *Interna-*

tional Journal of Heat and Mass Transfer, 53(9-10):2183–2192, 2010. ISSN 00179310. doi: 10.1016/j.ijheatmasstransfer.2009.12.020.

[25] G. Odabaşi. *Modeling of multidimensional heat transfer in a reactangular grooved heat pipe*. PhD Thesis, Middle East Technical University, 2014.

[26] P. C Wayner Jr and P. C. Wayner. The effect of interfacial mass transport on flow in thin liquid films. *Colloids and Surfaces*, 52:71–84, 1991. ISSN 01666622. doi: 10.1016/0166-6622(91)80006-A.

[27] J. A. Schonberg, S. DasGupta, and P. C. Wayner. An augmented Young-Laplace model of an evaporating meniscus in a microchannel with high heat flux. *Experimental Thermal and Fluid Science*, 10(2):163–170, 1995. ISSN 08941777. doi: 10.1016/0894-1777(94)00085-M.

[28] L. Biswal, S. K. Som, and S. Chakraborty. Thin film evaporation in microchannels with interfacial slip. *Microfluidics and Nanofluidics*, 10(1): 155–163, 2011. ISSN 16134982. doi: 10.1007/s10404-010-0655-7.

[29] S. Narayanan, A. G. Fedorov, and Y. K. Joshi. Interfacial transport of evaporating water confined in nanopores. *Langmuir*, 27(17):10666–10676, 2011. ISSN 07437463. doi: 10.1021/la201807a.

[30] L. Bai, G. Lin, and G. P. Peterson. Evaporative Heat Transfer Analysis of a Heat Pipe With Hybrid Axial Groove. *Journal of Heat Transfer*, 135(3): 031503, 2013. ISSN 0022-1481. doi: 10.1115/1.4022996.

[31] T. Kaya, G. Ball, J. Polansky. Investigation of particular features of the numerical solution of an evaporating thin film in channel. 013002:1–9, 2013. doi: 10.5098/hmt.v4.1.3002.

[32] S. Pati, S. K. Som, and S. Chakraborty. Combined influences of electrostatic component of disjoining pressure and interfacial slip on thin film evaporation in nanopores. *International Journal of Heat and Mass Transfer*, 64: 304–312, 2013. ISSN 00179310. doi: 10.1016/j.ijheatmasstransfer.2013.04.049.

[33] L. Biswal, S. K. Som, and S. Chakraborty. Thin film evaporation in microchannels with slope- and curvature-dependent disjoining pressure. *International Journal of Heat and Mass Transfer*, 57(1):402–410, 2013. ISSN 00179310. doi: 10.1016/j.ijheatmasstransfer.2012.10.022.

[34] H. B. Ma, P. Cheng, B. Borgmeyer, and Y. X. Wang. Fluid flow and heat transfer in the evaporating thin film region. *Microfluidics and Nanofluidics*, 4(3):237–243, 2008. ISSN 16134982. doi: 10.1007/s10404-007-0172-5.

[35] J. J. Zhao, Y. Y. Duan, X. D. Wang, and Bu X. Wang. Effect of nanofluids on thin film evaporation in microchannels. *Journal of Nanoparticle Research*, 13(10):5033–5047, 2011. ISSN 13880764. doi: 10.1007/s11051-011-0484-y.

[36] F W. Holm and S P. Goplen. Heat Transfer in the Meniscus Thin-Film Transition Region. *Journal of Heat Transfer*, 101(8):543–547, 1979. ISSN 00221481. doi: 10.1115/1.3451025.

[37] L. M. Hocking. The influence of intermolecular forces on thin fluid layers. *Physics of Fluids A: Fluid Dynamics*, 5(4):793–799, 1993.

[38] A. Indeikina and H -C. Chang. *A Molecular Theory for Dynamic Contact Angles*, pages 321–337. Springer Netherlands, Dordrecht, 1999. ISBN 978-94-011-4736-1. doi: 10.1007/978-94-011-4736-1_28.

[39] Q. Wu and H. Wong. A slope-dependent disjoining pressure for non-zero contact angles. *Journal of Fluid Mechanics*, 506(April 2004):157–185, 2004. ISSN 0022-1120. doi: 10.1017/S0022112004008420.

[40] B. Dai, L. G. Leal, and A. Redondo. Disjoining pressure for nonuniform thin films. *Physical Review E - Statistical, Nonlinear, and Soft Matter Physics*, 78(6):1–9, 2008. ISSN 15393755. doi: 10.1103/PhysRevE.78.061602.

[41] S. Moosman and G.M. Homsy. Evaporating menisci of wetting fluids. *Journal of Colloid and Interface Science*, 73(1):212–223, 1980. ISSN 00219797. doi: 10.1016/0021-9797(80)90138-1.